JOURNAL OF CAVE AND KARST STUDIES

Journal of Cave and Karst Studies

Volume 61 Number 1 April 1999

CONTENTS

Articles

Cover: Snottites (photo by J.A. Pisarowicz). See Hose and Pisarowicz page 13

ESTIMATES OF POPULATION SIZE OF *STYGOBROMUS EMARGINATUS* (AMPHIPODA: CRANGONYCTIDAE) IN A HEADWATER STREAM IN ORGAN CAVE, WEST VIRGINIA

SHANNON M. KNAPP[1] AND DANIEL W. FONG[2]
Department of Biology, American University, Washington, D.C. 20016 USA

Population sizes of Stygobromus emarginatus *were estimated using mark-recapture data at three sites each in two habitats of a headwater stream in the Organ Cave drainage. The stream channel habitat contained an average of 10 to 14 individuals per meter length and an estimated population size of 3000 to 4200 individuals. The pool habitat yielded very low recapture rates. We argue that the pool habitat represents a window into the epikarstic zone, and the low recapture rates indicate a large hidden population in the epikarst.*

A fundamental aspect of the ecology of organisms is population size. Small population size and small number of populations are typical reasons for a species to be listed as endangered or threatened. Although there are 50,000 to 100,000 obligate cave-dwelling species (Culver & Holsinger 1992), population sizes of only a few have been estimated using methods such as mark-recapture (see summary in Culver 1982; Simon 1997) that can provide more reliable results than simple sightings or one time counts. In this paper, we present initial results from a long term continuing study, initiated in September, 1994, to monitor fluctuations in population size of the crangonyctid amphipod crustacean *Stygobromus emarginatus* (Hubricht) in a headwater stream in Organ Cave, Greenbrier County, West Virginia.

STUDY ORGANISM AND STUDY SITE

We chose to monitor the population size of *S. emarginatus* for several reasons. First, as is typical of most troglobites, little is known about its basic ecology. Second, its large body size at maturity, up to 10 mm for males and 14 mm for females (Holsinger 1972), renders it amenable to mark-recapture studies. Third, one time count estimates indicate that populations of *S. emarginatus* occur at densities of 15/m² (Holsinger *et al.* 1976) to 30/m² (Culver *et al.* 1994), densities that may yield meaningful recapture rates in a mark-recapture study. Finally, Fong and Culver (1994) showed that within the Organ Cave system, *S. emarginatus* mainly occurs in small headwater streams, and is absent in large streams in the lower reaches of the cave drainage. They hypothesized that the primary habitat of *S. emarginatus* is not in the cave stream, but rather is in the interstitial water in the epikarst, the highly fractured limestone interface with the soil (Williams 1983). Their hypothesis predicts that the population size of *S. emarginatus* in cave streams

near the epikarst should covary with the amount of water input from the epikarst into the cave stream. A long term study of the population size of this species should provide baseline data that eventually can be used to test this hypothesis.

Sively #2 is a headwater stream in the eastern section of Organ Cave (Stevens 1988). The stream originates as percolating water seeps and drips into the upstream portion of the cave passage, and flows for ~300 m before it sinks into breakdown. Two distinct habitats are associated with the stream: the rock-bottomed stream channel and mud-bottomed pools adjacent to the stream channel. The average width of the main channel is about 0.5 m. The pools occur in the upper reaches of the stream, are fed by seeps and also by water from the stream channel during high water, and frequently dry up completely. These pools average about 1.2 m in diameter. Depth of the water is typically less than 10 cm at all habitats. We picked this stream as the study site because it is easily accessible, it appears to have significant water input from the epikarst, especially in its upper half, and, based on complete dissection of 12 riffles, it contains *S. emarginatus* at a density of 11.5/ m² (Culver *et al*. 1994).

METHODS

We estimated the population size of *S. emarginatus* in late October, 1994 (OCT94), during the dry season; in mid-January and early April, 1995 (JAN95 and APR95), during the wet season; and in late June, 1995 (JUN95), during the beginning of the dry season. We designated six sampling sites in the Sively #2 stream, chosen primarily by the ease of access to the water. The sites were numbered sequentially from the downstream end. Sites S1, S2 and S3 were located in the stream channel at the lower half of the stream. Flow in the stream channel was intermittent in the upper half of the stream. Each stream site consisted of a 6-10 m length of the stream, and was separated from other sites by at least 15 m. Sites P4, P5 and P6 were mud-bottomed pools adjacent to the stream channel in the upper half of the stream. These pools ranged from 1.0 m to 1.5

---

[1] Present address: Department of Fisheries and Wildlife Biology, Virginia Polytechnic Institute and State University, Blacksburg, VA 24061
[2] Corresponding author.

m in diameter.

During each sampling period at each site, we took two samples of *S. emarginatus* at an interval of twenty-four hours. A sample consisted of all specimens collected individually with a turkey baster until the rate of finding additional animals had substantially diminished, a duration of about three to five worker-hours. After the first sample, we placed each specimen on a paper towel to absorb excess water, marked its tergum on the thorax with a blue or red Sharpie® permanent ink marker, and immediately put it in a dish of water. No animal was out of the water for more than 10 seconds. When all specimens had been processed, we confirmed that all individuals in the water dish were obviously marked and were able to walk or swim about before releasing them. After the second sample, we tallied the number of marked and unmarked individuals and released the specimens. We marked all specimens at all sites with blue ink in OCT94, and with red ink in JAN95. In APR95 and in JUN95, we marked individuals at odd numbered sites with blue ink and those at even numbered sites with red ink. Preliminary trials using this technique in the laboratory induced no mortality, with five of six specimens having retained the markings for over six months while the sixth lost its marking upon molting after four months.

We estimated population size using the Lincoln-Peterson index:

$$N = a\,n\,/\,r\,, \quad S.E. = [a^2\,n\,(n-r)\,/\,r^3 + 1]^{0.5}$$

or the Bailey correction for low numbers of recaptures ($r \leq 20$):

$$N = a\,(n+1)\,/\,(r+1), \quad S.E. = [a^2\,(n+1)\,(n-r)\,/\,(r+1)^2\,(r+2)]^{0.5}$$

where N is the estimated population size and S.E. is the standard error of the estimate, a is the number of specimens marked and released in the first sample, n is the total number in the second sample, and r is the number of recaptures in the second sample (Begon 1979). For comparisons among sites and among seasons, density expressed as estimated population size per unit stream length (N/m) was used for stream sites. This was a more consistent index of density than estimated population per unit stream area (N/m²) because of the shallow nature of the stream channel, where a slight change in depth resulted in a drastic change in the surface area measured along the same length of stream.

RESULTS

We did not recapture any specimen marked during any previous estimation (Table 1). In APR95 and JUN95, when specimens from adjacent sites were marked with different colors, we did not recapture any color-mismatched specimens at any site.

Table 1. Mark-recapture data for *S. emarginatus* in Sively #2 stream in Organ Cave. a: number marked and released; n: number in second sample; r: number of recaptures; N and S.E.: estimated population size and standard error; N/m: estimated density per meter stream length.

		Stream Sites				Pool Sites			
Date		S1	S2	S3	Total	P4	P5	P6	Total
OCT94	a	29	10	15	54	-	-	-	-
	n	32	21	45	98	-	-	-	-
	r	14	3	5	22	-	-	-	-
	N	64	55	115	241	-	-	-	-
	S.E.	12	22	40	45				
	N/m	10	12	18	14				
JAN95	a	38	32	-	70	44	23	22	89
	n	42	35	-	77	27	17	14	58
	r	13	6	-	19	1	2	0	3
	N	117	165	-	273	616	138	-	1313
	S.E.	25	52	-	51	343	63	-	567
	N/m	6	16		10				
APR95	a	52	30	15	97	-	11	10	21
	n	55	33	20	108	-	6	2	8
	r	22	15	6	43	-	0	0	0
	N	130	64	45	244	-	-	-	-
	S.E.	22	11	13	29	-	-	-	-
	N/m	16	9	6	11				
JUN95	a	46	25	21	92	-	-	-	-
	n	48	31	10	84	-	-	-	-
	r	15	12	5	36	-	-	-	-
	N	141	61	38	215	-	-	-	-
	S.E.	28	13	10	27	-	-	-	-
	N/m	18	8	5	10				

STREAM SITES

We were able to estimate population sizes at all stream sites during all four sampling periods except one. In JAN95, we mistakenly sampled longer segments of the stream at S1 and S2 than originally planned, completely overlapping the original S3 site. The total distance sampled at S1 and S2 in JAN95, however, was similar to the total distance sampled at all three sites during the other three estimation periods.

Among stream sites, we marked an average of 28 specimens per site per estimation period, with a range of 10 to 52. The sizes of the second samples were generally similar, and ranged from 10 to 55 but averaged slightly higher at 34. Recapture rates (r/a in Table 1) ranged from 19% to 50%, with an average of 36%. Estimated population sizes ranged from 38 to 165 per site per estimation period, and averaged 90. Corresponding densities ranged from 5/m to 18/m, and averaged 11/m. Combining the data from all three sites for each estimation period resulted in estimated population sizes from 215 to 273 with an average of 254. The combined data yielded corresponding densities from 10/m to 14/m, with an average

of 11/m which was identical to the average of the separate sites.

We used the estimated density per stream length to gauge the population size of *S. emarginatus* in the stream channel. Because of the apparent lack of migration of specimens among stream sites, we treated the values obtained from each site as independent estimates and calculated their mean. The average density values were 13.3/m, 11.0/m, 10.3/m, and 10.3/m, respectively, for OCT94, JAN95, APR95, and JUN95. These mean values closely matched the corresponding values based on combining the data from the three sites, at 14/m, 10/m, 11/m, and 10/m. Thus, assuming that the three sites are representative of the entire stream, we estimated that the population size of *S. emarginatus* in the channel of the Sively #2 stream, at a mapped length of about 300 m, was between 3000 and 4200 individuals.

POOL SITES

We were able to estimate population sizes at only two pool sites, P4 and P5, in JAN95. In OCT94, all three pools held little water and were not sampled. In JAN95, P6 yielded no recaptures from 22 marked specimens. In APR95, P4 was completely dry while P5 and P6 had shrunk to 20% of their sizes in JAN95, and we obtained no recaptures from 21 specimens marked in P5 and P6 combined. All three pools were completely dry in JUN95.

Among pool sites, we marked an average of 22 animals per pool per estimation period, with a range of 10 to 44. The second samples, however, were consistently smaller than the first samples, and ranged from two to 27 with an average of only 13. The recapture rates were extremely low, at 3% for all three pools combined in JAN95, and there were no recaptures in APR95. Estimated population sizes for sites P4 and P5 in JAN95 were 616 and 138, respectively. Combining the data from all three pools in JAN95 yielded an estimate of 1313. The standard errors for all these estimates were large due to the small numbers of recaptures.

OVIGEROUS FEMALES

We were unable to obtain sex ratios of the specimens because *S. emarginatus* was difficult to sex accurately without examination under the microscope. We were able to identify ovigerous females by the presence of developing embryos in their ventral marsupia. The proportion of ovigerous females among individuals captured at a site ranged from 3% to 18% from stream sites and from 4% to 25% from pool sites (Table 2). Combined data from stream sites showed the proportion of ovigerous females at 6%, 9%, 11%, and 4%, respectively, for OCT94, JAN95, APR95, and JUN95. Corresponding values for pool sites were 9% in JAN95 and 3% in APR95. There were too few values, however, to identify possible seasonal trends. Among stream sites, ovigerous females seemed to congregate disproportionately at one of the three sites. S1, the most downstream site, accounted for between 82% to 100% of the ovigerous females during any estimation period. Although

Table 2. Occurrence of ovigerous females of *S. emarginatus* in Sively #2 stream in Organ Cave. O: number of ovigerous females; T: total number of different individuals sampled (= a + n - r of Table 1); p: ovigerous females as proportion of individuals sampled (= O/T).

Date		Stream Sites				Pool Sites			
		S1	S2	S3	Total	P4	P5	P6	Total
OCT94	O	8	0	0	8	-	-	-	-
	T	47	28	55	130	-	-	-	-
	p	0.17	0.00	0.00	0.06	-	-	-	-
JAN95	O	9	2	-	11	3	1	9	13
	T	67	61	-	128	70	38	36	144
	p	0.13	0.03	-	0.09	0.04	0.03	0.25	0.09
APR95	O	15	2	0	17	-	1	0	1
	T	85	48	29	162	-	17	12	29
	p	0.18	0.04	0.00	0.11	-	0.06	0.00	0.03
JUN95	O	6	0	0	6	-	-	-	-
	T	79	44	26	140	-	-	-	-
	p	0.08	0.00	0.00	0.04	-	-	-	-

ovigerous females were found in sufficient numbers among pool sites only in JAN95, nine of the 13 specimens were also concentrated in one site, P6.

DISCUSSION

Results from this study show that the mark-recapture technique used can provide accurate data on estimating population sizes of stygobites such as amphipods in caves. Some individuals could have lost their markings upon molting between the first and second samples during each estimation period. The magnitude of this error is likely small because of the short interval between samples and because molting in *Stygobromus* is infrequent, as molting is rarely observed among specimens kept over long periods in the laboratory. The lack of recapture of color mis-matched specimens when specimens from adjacent sites were marked with different colors indicates that, at least during the 24 hour sampling interval, there was no significant migration of individuals among sites. For stream sites, the sizes of the first and second samples were generally similar, indicating equal sampling efforts. These results, in combination with the high average recapture rate of 36%, indicate that the estimated values, of density between 10/m to 14/m and population size in the stream channel between 3000 and 4200, are reasonable.

For pool sites, low recapture rates inflated the standard errors of the population size estimates. We suggest that these low recapture rates, compared to the relatively high rates at

stream sites, may reflect a complex three-dimensional nature of the pool habitat, that beneath the soft muddy substrate water in these pools communicates with water in the epikarst. These pools thus represent small windows into the epikarst, and fill when water in the epikarst expand during wet periods, and dry up when water in the epikarst contract during dry spells. Animals found in these pools may thus comprise a small sample of a larger population inhabiting the epikarst. Although our data indicate that *S. emarginatus* do not migrate far in 24 hours, marked specimens need only cover short distances to move out of these small and shallow pools. We did observe one marked specimen that burrowed and disappeared into the mud bottom of P5 in JAN95, and it did not reappear before we gave up after waiting for 20 minutes. The low recapture rates thus resulted from our having marked only a small portion of the population. We suggest that the estimated population size of 1313 from the pool habitat in JAN95, although not highly reliable, does point to a potentially large hidden population. Further study at these pool sites will need to employ different techniques, such as removal sampling over several days during the wet season, to estimate population size in this habitat.

The consistent preponderance of ovigerous females at S1 among stream sites during all four estimation periods, and the concentration of ovigerous females in P6 among pool sites in JAN95, indicate probable strong microhabitat preference by ovigerous females and uneven distribution of microhabitats among sites. Our experience during sampling was that all individuals were clumped within stream sites, and that usually several specimens were captured within short periods separated by long spans when no specimens were found, again suggesting strong microhabitat preference.

REFERENCES

Begon, M. (1979). *Investigating Animal Abundance: Capture-Recapture for Biologists*. University Park Press. Baltimore, MD.

Culver, D.C. (1982). *Cave Life: Ecology and Evolution*. Harvard University Press. Cambridge, MA.

Culver, D.C. & Holsinger, J.R. (1992). How many species of troglobites are there? *National Speleological Society Bulletin 54*: 79-80.

Culver, D.C., Jones, W.K., Fong, D.W. & Kane, T.C. (1994). Organ Cave karst basin. In Gibert, J., Danielopol, D. & Stanford, J. [eds.]. *Groundwater Ecology*. Academic Press. San Diego, CA: 451-473.

Fong, D.W., & Culver, D.C. (1994). Fine-scale biogeographic differences in the crustacean fauna of a cave system in West, Virginia, USA. *Hydrobiologia 287*: 29-37.

Holsinger, J.R. (1972). *The Freshwater Amphipod Crustaceans (Gammaridae) of North America*. Biota of Freshwater Ecosystems Identification Manual No. 5. EPA. Washington, D.C.

Holsinger, J.R., Baroody, R.A. & Culver, D.C. (1976). *The Invertebrate Cave Fauna of West Virginia*. Bulletin No. 7, West Virginia Speleological Survey. Barrackville, WV.

Simon, K.S. (1997). Effects of organic pollution on an Appalachian cave: changes in macroinvertebrate populations and food supplies. *American Midland Naturalist 138*: 387-401.

Stevens, P.J. (1988). *Caves of the Organ Cave Plateau, Greenbrier County, West Virginia*. Bulletin No. 9, West Virginia Speleological Survey. Barrackville, WV.

Williams, P.W. (1983). The role of the subcutaneous zone in karst hydrology. *Journal of Hydrology 61*: 45-67.

A LABORATORY INVESTIGATION OF THE RELATIVE DISSOLUTION RATES OF THE LIRIO LIMESTONE AND THE ISLA DE MONA DOLOMITE AND IMPLICATIONS FOR CAVE AND KARST DEVELOPMENT ON ISLA DE MONA

MYRNA IRIS MARTINEZ[1] AND WILLIAM B. WHITE[2]

Department of Geosciences, The Pennsylvania State University, University Park, PA 16802 USA

The relative dissolution kinetics of the Lirio Limestone and the Isla de Mona Dolomite were determined by dissolving discs of various samples in CO_2-saturated solutions. Rate curves for carbonate dissolution were determined by monitoring pH and specific conductance as a function of time. Dissolution rates for limestone samples were distinctly higher than rates for dolomite samples but the rate curves had similar shapes. Initial rates for limestones averaged 12.53 $\mu mol\ m^{-2}\ sec^{-1}$ compared with 8.53 for dolomite. The limestone rates are comparable with those measured on single crystal calcite but the dolomite rates are higher than rates measured on Paleozoic dolomites. The relative dissolution rates are sufficient to be a factor in explaining the concentration of caves at the limestone/dolomite contact but may not be the only controlling factor.

Isla de Mona is a 6-km wide carbonate island located in the deep water of the Mona Passage about halfway between Puerto Rico and the Dominican Republic. Except for small beach areas on the south side, the island is bounded by cliffs rising up to 90 m msl. The main portion of the island is a karst plateau underlain by the Miocene Lirio Limestone. The core of the island is composed of the Isla de Mona Dolomite (Kaye 1959; Frank *et al.* 1998a). There are many caves on the island, mostly located on the plateau escarpment near the contact between the limestone and the dolomite (Frank 1993; Frank *et al.* 1998b).

There is a marked contrast in the response to dissolution of the Lirio Limestone and the Isla de Mona Dolomite. The Lirio Limestone comprises most of the plateau surface and is breached to expose the underlying dolomite only at the large closed depression of Bajura de los Cerezos (Briggs & Seiders 1972). Elsewhere, the Isla de Mona Dolomite is exposed at the surface only on the sea cliffs. The Lirio Limestone is sculptured into a complex karren surface on much of the plateau and is penetrated by many shafts. As far as has been observed the shafts splay out into short horizontal dissolution openings at the limestone/dolomite contact. They do not penetrate significantly into the dolomite (Frank 1993). Likewise, cave development is largely limited to the basal Lirio Limestone. Accepting the hypothesis that the large caves on Isla de Mona are mixing zone caves (Frank *et al.* 1998b), there remains the problem of why there are so few caves in the dolomite. Interpretation of the groundwater flow system on Isla de Mona depends strongly on whether or not conduits occur deep within the dolomite, perhaps as drains to the coast during low stands of sea level. So far, evidence for any type of conduit permeability at or below the present water table is sparse. Only Cueva del Agua de Puenta Brava, at the base of the sea cliff, reaches to the water table.

In the Paleozoic carbonate rocks of the Appalachians, dolomites tend to exhibit substantially less karst development than do limestones (Rauch & White 1970). Limestone surfaces may exhibit deep closed depressions while nearby dolomite terrain exhibits only shallow swales. Large caves and integrated drainage systems develop in the limestones; caves range from small to nonexistent in the dolomites. This contrast arises from the substantially different rates of dissolution of calcite and dolomite, and one must entertain the hypothesis that similar lithologic controls may operate on Isla de Mona. It must be demonstrated, however, that the Miocene carbonate rocks of Isla de Mona with their high primary permeability do, in fact, function in a geochemically similar way to the dense, low permeability Paleozoic carbonates of eastern United States.

The objective of this investigation was to compare the dissolution kinetics of the Lirio Limestone and the Isla de Mona Dolomite by means of a quantitative laboratory investigation. The rates of dissolution of selected samples of Lirio Limestone and Isla de Mona Dolomite were measured in CO_2-saturated water. These results then can be compared with other investigations of calcite and dolomite dissolution.

---

[1] Present address: 100 Carmen Hills Drive, Box 141, San Juan, Puerto Rico 00926; myrna_isis@yahoo.com

[2] Also affiliated with The Materials Research Laboratory.

Sample Selection and Characterization

Kilogram size samples of both rock formations were collected at several locations on the island. The mineral compositions of these samples were determined by X-ray powder diffraction. Sample locations and mineral identifications are given in Table 1.

Acetate peels were prepared in duplicate for each sample. One of each of the duplicates was stained using a combination of Alizarin Red-S and potassium ferricyanide stains. Pink to red color indicates calcite, mauve to blue indicates ferroan calcite, no color indicates dolomite, and a very pale blue indicates ferroan dolomite. All peels were studied with a petrographic microscope.

LLC: The rock is white, with a fine-grained matrix, and is composed of at least 50% allochems. All allochems are fossils, mainly corals. Well preserved gastropods can be seen. Most of the rock stained a deep pink color in confirmation of the x-ray results.

LLL: The rock is very dense, fine-grained limestone with low porosity. The color is white to beige. The only fossils that can be easily recognized are corals, some of which are crystalline, an indication of calcite replacement. The rock stained from light to dark pink.

LLVC: The rock shows strong evidence of dolomitization. Although the geologic map shows the collection area as limestone, the collection point at the bottom of a 10-m pit is apparently in a transition zone between limestone and dolomite. The x-ray pattern indicates somewhat less than half of the sample is calcite while the remainder is dolomite. The more continuous matrix did not stain. About 50-70% of the observable crystals were very well defined dolomite rhombs.

MDB: The rock was cream to bone white. The matrix was fine-grained, fairly massive with a large vuggy porosity. Small fossils are abundant, particularly bivalve shells and pieces of coral. The larger fossils have been dissolved and have been replaced by crystals visible with a hand lens. The bulk rock was unstained in agreement with x-ray results indicating that most of the rock was dolomite. Some of the larger grains stained pink. Most of the fossils were only partially stained, indicating only partial replacement of the original shell material. Some vuggy porosity can still be seen under the microscope and some calcite cement is still present.

MDL: The rock is very fine-grained with a sugary texture. It has some vuggy and moldic porosity. Most of the recognizable fossils are corals. The rock picked up a very light pink stain and there are some patches of calcite scattered in the matrix. The calcite was not detected by x-ray which showed only a well-crystallized and well-ordered dolomite.

Although dissolution experiments were performed on all five rock samples, LLC and LLL were taken as monomineralic limestones while MDL was the closest to a monomineralic dolomite so that these specimens should give the strongest contrast in dissolution kinetics.

Table 1. Location and Description of Rock Specimens

Code	Rock Type	Location	Mineralogy*
LLC	Lirio Limestone	Plateau surface near Cueva El Capitan	Calcite
LLL	Lirio Limestone	Cliff face below Cueva del Lirio	Calcite
LLVC	Lirio Limestone	Bottom of pit, along trail to Bajura de los Cerezos. 10 m below surface, near Lirio/Mona contact.	40% calcite / 60% dolomite
MDB	Mona Dolomite	Northwest corner of island between Punte Capitan and Cabo Noroeste.	90% dolomite / 10% calcite
MDL	Mona Dolomite	At sea level below Cueva del Lirio	Dolomite

*Mineral percentages determined from relative intensities of X-ray diffraction lines.

Experimental Methods

The experimental procedure followed those developed earlier in this laboratory by Herman (1982; Herman & White 1985). The rock specimens were sawed into slabs about 12 mm thick. Circular disks about 40 mm in diameter were cut from the slabs with a diamond core drill. These were mounted in a chuck and sealed so that only one face of the disk was exposed to the solution. The effective diameter of each disk was measured with calipers. The apparatus for the dissolution experiments is sketched in figure 1. It consists of a vessel containing 800 mL of solution held in a constant temperature bath at 25°C. The sample in its chuck was attached by a drive shaft to a gear box that allowed the sample disk to be spun at various angular velocities. Also inserted into the solution was a conductivity probe and a pH electrode. The solution was continuously saturated with CO_2 bubbled from a tank through a fritted glass disperser.

The spinning disk technique allows dissolution to take place with constant mass transfer across the surface of the disk (Levich 1962). For these experiments a single rotation rate of 225 rpm was chosen. This corresponds to a Reynolds number of 11,200 at 25°C.

Both pH and specific conductance measurements were recorded at specific time intervals. Data were recorded every hour in the early stages of a dissolution run and every few hours as the experiment progressed. Total run times were about five days. All runs were made in duplicate. Samples of 1.0 mL or less were drawn eight times in the course of each run and analyzed for Ca and Mg by atomic emission spectroscopy. These analyses allowed the determination of the relation between specific conductance and hardness specifically calibrated for the Isla de Mona rocks.

Results

Background Chemistry and Data Processing

The gas bubbled through the solution was pure CO_2 saturated with water vapor. Because the solution was kept constantly saturated with CO_2, it behaves as an open system with a constant P_{CO_2}. Taking account of the elevation of the laboratory (350 m) and deducting the contribution from the vapor
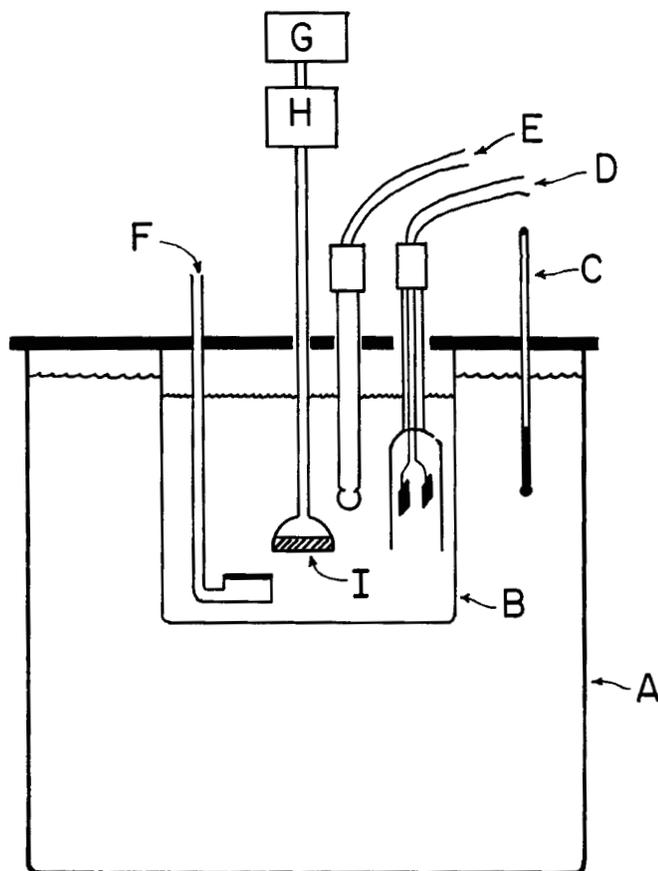
Figure 1. Schematic drawing of experimental apparatus. A = constant temperature bath set at 25°C. B = beaker containing 800 mL of aqueous solution. C = thermometer. D = Conductivity electrode. E = pH electrode. F = CO_2 inlet through fitted glass disk. G = drive motor. H = gear reduction box. I = disk of experimental sample.

pressure of water, $P_{CO_2} = 0.93$ atm for all experiments.

By assuming equilibrium among the dissolved CO_2, $H_2CO_3^{\circ}$, and HCO_3^-, before the disk was inserted, the initial pH was calculated to be 3.93, in good agreement with the measured value. If the dissolution reaction was assumed to go to equilibrium, the final pH was calculated, using equations derived by Drever (1997), to be 5.93.

Dissolved Ca + Mg concentrations in units of millimoles/liter, as determined by chemical analysis, were plotted against the corresponding values for specific conductance, Spc (Fig. 2). There is a surprising amount of scatter. Hardness/conductance plots of spring waters typically exhibit varying degrees of scatter because of variations in other constituents of the water. Laboratory investigations usually produce very tight fits of the data. The source of the scatter is not known but the scatter reduces the precision with which Ca + Mg can be measured. Fitting a linear regression to the data in figure 2 gives the result:
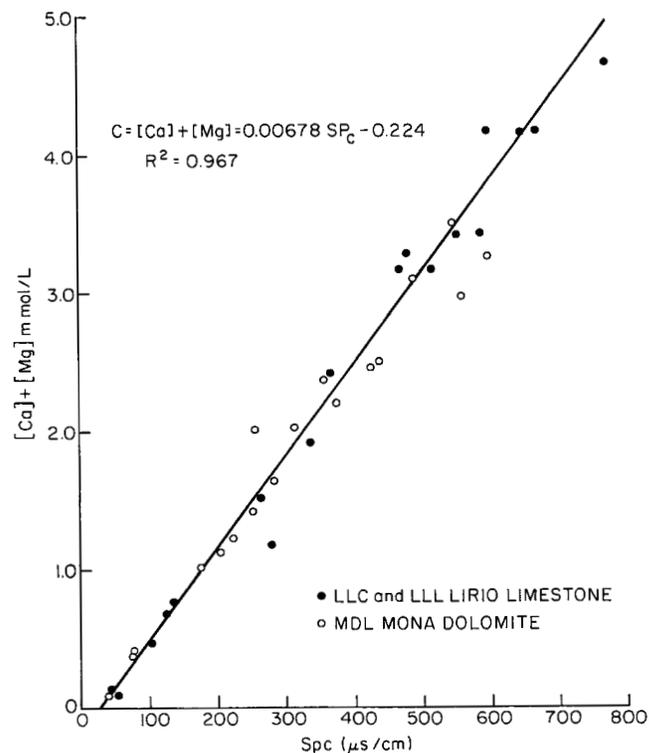
Figure 2. Relation of [Ca] + [Mg] determined by atomic emission spectroscopy to specific conductance for limestone and dolomite samples. Solid line represents the linear regression of all data points.

$$[Ca] + [Mg] = 0.00678Spc - 0.244 \qquad [1]$$

where concentrations are given in millimoles/liter. Limestone and dolomite data are very similar so that a single regression was fitted to both data sets. Equation [1] was used to extract [Ca] + [Mg] from specific conductance data collected during the kinetics experiments.

The overall reactions for dissolution of calcite and dolomite are:

$$CaCO_3 + CO_2 + H_2O \iff Ca^{2+} + 2HCO_3^-$$

$$CaMg(CO_3)_2 + 2CO_2 + 2H_2O \iff Ca^{2+} + Mg^{2+} + 4HCO_3^-$$

Charge neutrality requires that:

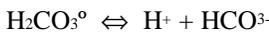$$[H^+] + 2[Ca^{2+}] = [HCO_3^-] \qquad [2]$$

which in terms of activities is:

$$\frac{a_{H^+}}{\gamma_{H^+}} + 2\frac{a_{ca^{2+}}}{\gamma_{Ca^{2+}}} = \frac{a_{HCO_3^-}}{\gamma_{HCO_3^-}} \qquad [3]$$

where a is activity of the given ion and γ is the activity coefficient.

If the reactions:

$$CO_2(gas) + H_2O \Leftrightarrow H_2CO_3^o$$

$$\frac{a_{H_2CO_3}}{P_{CO_2}} = K_{CO_2} \qquad [4]$$

$$H_2CO_3^o \Leftrightarrow H^+ + HCO_3^-$$

$$\frac{a_{H^+} \, a_{HCO_3^-}}{a_{H_2CO_3}} = K_1 \qquad [5]$$

are assumed to be in equilibrium (a good assumption on the time scale of these experiments), the bicarbonate activity for a system open to CO_2 is given by:

$$a_{HCO_3^-} = \frac{K_1 K_{CO_2} P_{CO_2}}{a_{H^+}} \qquad [6]$$

where the Ks are the equilibrium constants for the given reactions.

Substituting equation [6] into equation [3] and rearranging terms provides the needed relationship for calculation of $[Ca^{2+}]$ from measured pH.

$$[Ca^{2+}] = \frac{1}{2}\left[\frac{K_1 K_{CO_2} P_{CO_2}}{\gamma_{HCO_3^-} a_{H^+}} - \frac{a_{H^+}}{\gamma_{H^+}}\right] \qquad [7]$$

The equation for dolomite is the same except that the calculation gives [Ca] + [Mg].

Equation [7] was used to extract the amount of dissolved Ca + Mg from the measured pH. The concentrations of [Ca] + [Mg] calculated from specific conductance were used to estimate ionic strength and thus to calculate the activity coefficient for the bicarbonate ion.

LIMESTONE AND DOLOMITE DISSOLUTION

Full rate curves for three pairs of samples, two limestones and one dolomite are shown in figure 3. These samples were selected because LLC and LLL were phase-pure calcite and MDL was close to a phase-pure dolomite. The reproducibility between runs is 10-20% but the scatter of individual data points is much smaller indicating that the mismatch between duplicate pairs is due to the heterogeneities of the rock samples themselves rather than error in the measurements. Sample LLC, in particular is a highly porous and vuggy limestone so that the effective surface area is much larger than the geometric area of the disk.
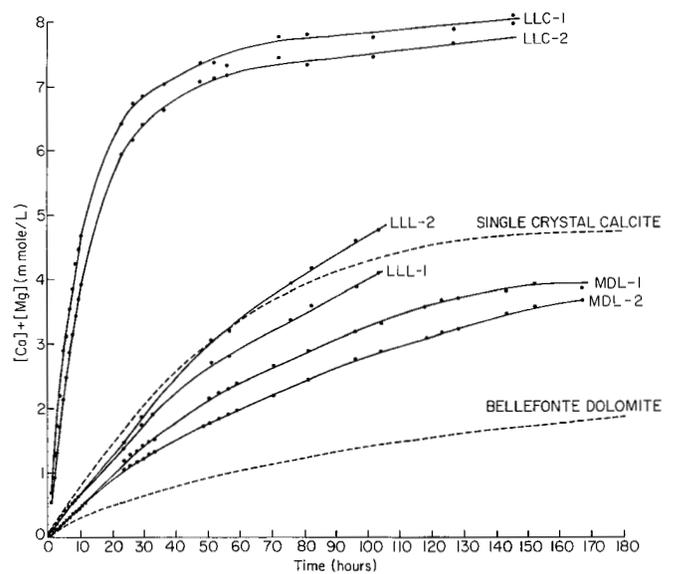

Figure 3. Dissolution rate curves for duplicate runs of samples LLC, LLL, and MDL. [Ca] + [Mg] of limestone samples determined from pH; [Ca] + [Mg] of dolomite sample determined from specific conductance. Single crystal calcite data (dashed curves) from Herman (1982).

The saturation concentration of $[Ca^{2+}]$ based on pure calcite at $P_{CO_2} = 0.93$ atm is calculated to be 8.145 mmol/L. Only sample LLC approaches saturation on the time scale of the experiments. The more massive limestone, LLL, dissolved rapidly but had reached only about half saturation at the termination of the experiment. The dolomite runs were continued longer but dolomite MDL had not approached equilibrium after 7 days.

INITIAL RATES

To compare the dissolution rates of one rock type with another, it is convenient to examine the initial rate when the solutions are far from equilibrium. The rate curves are essentially linear over the first 10 hours of the experiments (Fig. 4) so that the initial rate can be described by:

$$\mathbf{Rate} = \frac{V}{A}\frac{dC}{dt} \qquad [8]$$

where V = volume of solution (800 mL in all experiments), A = area of exposed face of disk, and dC/dt is the slope of the near-linear plot of concentration against time. The data for each experimental run were fitted by linear regression of the data to obtain dC/dt for each experiment. The experimental data were collected with [Ca] + [Mg] in units of mmol/L and time in hours. These units were converted to calculate the initial rates in units of μmol m^{-2} sec^{-1} (Table 2). The lines in figure 4 are linear regressions using data for duplicate runs of each of the rock samples.
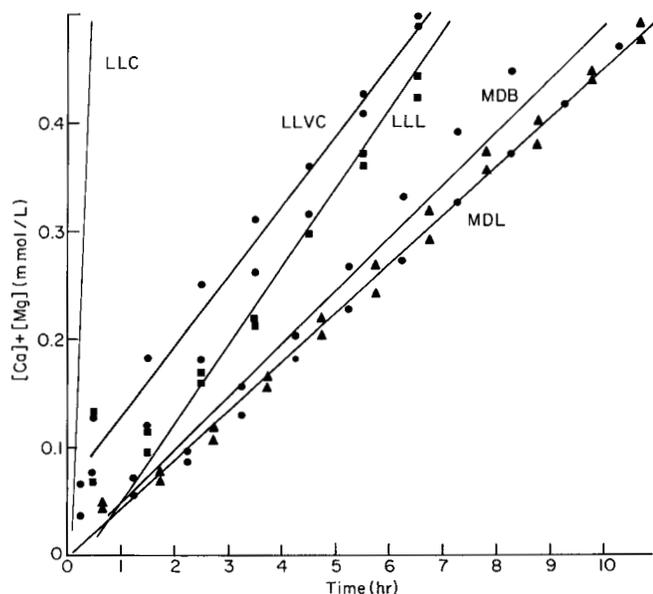
Figure 4. Initial dissolution rates for all samples. Solid lines represent linear regressions through both duplicate run data sets for each sample. Data points for LLC fall off the scale on this plot.

Table 2. Initial Dissolution Rates.

Sample Code	A (cm²)	dC/dt (mol/L-hr)	Rate (μmol m^{-2} sec^{-1})
LLC-1	12.24	0.420	76.24
LLC-2	12.13	0.361	66.13
LLL-1	12.55	0.0766	13.56
LLL-2	12.45	0.0704	12.57
LLVC-1	12.19	0.0703	12.81
LLVC-2	12.19	0.0610	11.12
MDB-1	12.25	0.0551	9.99
MDB-2	12.16	0.0435	7.95
DMDB-1	12.25	0.0450	8.16
DMDB-2	12.16	0.0473	8.64
MDL-1	12.18	0.0450	8.21
MDL-2	12.34	0.0457	8.23
Calcite*	12.74	-.----	11.66
Dolomite*	13.33	-.----	4.11

*Single crystal calcite and Bellefonte (Ordovician) dolomite from data of Herman (1982).

CALCIUM/MAGNESIUM RATIOS

Dissolution of the dolomite sample MDL gives values of [Ca]/[Mg] of 1.61 for the first run and 1.47 for the second run. These ratios do not change as the experiment progresses. The solutions are somewhat more calcium-rich than expected for a stoichiometric dolomite but consistent with the petrologic examination which suggests some calcite in the dolomite. In contrast, the [Ca]/[Mg] ratio changes continuously as the limestone specimens were dissolved (Fig. 5). Both runs on specimen LLL are plotted. The concentration of magnesium in solution is in the range of 0.5 to 1.5 mg/L, resulting in large analytical uncertainties and corresponding scatter in the ratios. The Ca^{2+} ion concentration increases as the dissolution reac-
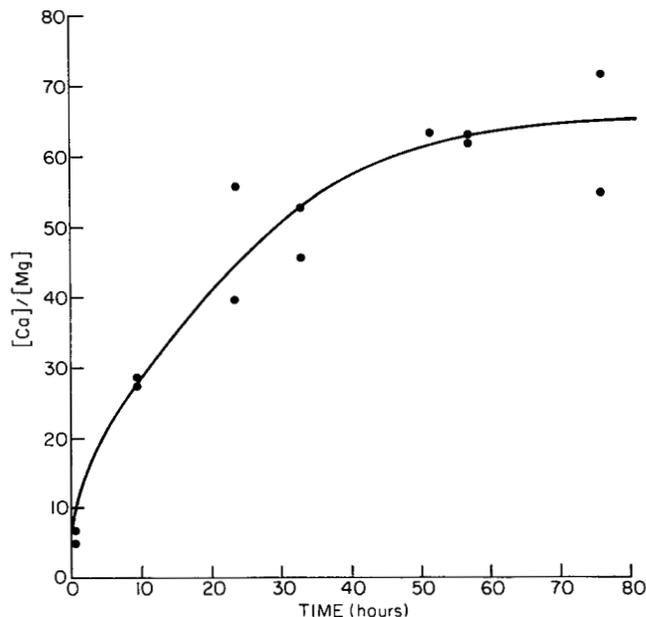
Figure 5. Change with time of [Ca]/[Mg] for limestone sample LLL.

tion proceeds whereas the Mg^{2+} ion concentration increases only slightly.

COMPARISON WITH LITERATURE DATA

A direct comparison can be made with the single crystal results of Herman (1982) because her study also used the spinning disk technique with nearly the same area disks. Herman found that dissolution rates under highly undersaturated conditions were strongly dependent on Reynolds number. Two of Herman's rate curves, one for single crystal calcite and one for the dense Ordovician Bellefonte Dolomite are drawn on figure 3. The agreement is excellent between the rate of dissolution of the Lirio Limestone (Sample LLL) and the single crystal calcite. In contrast, the rate of dissolution of the Isla de Mona Dolomite is about twice the rate of dissolution of the Bellefonte Dolomite. Mineralogic and lithologic examination of the Isla de Mona Dolomite reveals a substantial quantity of calcite interspersed with a well-ordered dolomite. It seems likely that the calcite is responsible for the high dissolution rate compared to the dense Paleozoic dolomite.

A set of experiments on the dissolution rate of Paleozoic limestones (Rauch & White 1977) used a different geometry. Solutions were pumped through holes drilled into limestone blocks. In spite of the difference in geometry, the results are similar to those obtained using the spinning disk technique.

Recent experimental results (Dreybrodt *et al.* 1996; Liu & Dreybrodt 1997) show that there are three rate-determining processes: reaction rate controlled kinetics at the mineral/water interface, mass transport by diffusion, and the slow kinetics of the hydration of dissolved carbon dioxide. As a result, the results of laboratory experiments conducted at high carbon

dioxide pressures must be applied with caution to natural systems where carbon dioxide pressures are usually much lower.

APPLICATION TO CAVE AND KARST DEVELOPMENT ON ISLA DE MONA

In broad terms, the caves of Isla de Mona fall into two categories: the large mixing-zone caves near the coast and shafts with minor caves scattered over the Plateau. The mixing zone caves and the splay passages at the bases of the shafts occur mainly at the contact between the limestone and dolomite. We can now turn to the question that this experimental investigation was intended to address. Can one account for the general absence of cave development in the dolomite solely in terms of a slower dissolution rate for the dolomite? The answer is that it is probably only part of the reason. The dolomite definitely dissolves more slowly than the limestone and this is part of the reason that cave development fades out at the contact. But the dissolution rate contrast is not as great as the rate contrast between Paleozoic limestones and dolomites.

There are no geochemical data on the infiltration waters on Isla de Mona. The soils on the Plateau are either thin or nonexistent. Rainfall on the Plateau has little opportunity to pick up CO_2 much beyond the atmospheric background. The aggressivity of the water, low to begin with, is quickly lost in the dissolution of the limestone surface in the Lirio Limestone. Water reaching the underlying dolomite would have a low CO_2 partial pressure and not be highly undersaturated. This factor would also contribute to the absence of conduit dissolution in the dolomite. Our proposed interpretation, based in part only on geologic evidence, is that it is a combination of slower kinetics and the CO_2-poor infiltration water that restricts cave development to the Lirio Limestone and the Lirio/Isla de Mona contact zone. In the absence of additional geochemical data, more precise interpretation is difficult.

CONCLUSIONS

Dissolution rates were measured on samples of Lirio Limestone and Isla de Mona Dolomite under experimental conditions of 25°C, $P_{CO_2} = 0.93$ atm, and Reynolds number = 11,200. Bulk limestone dissolved at about the same rate as single crystal calcite. The high porosity and thus high surface area of some limestones creates greatly enhanced apparent dissolution rates. The dissolution rate of the Mona Dolomite was about half the dissolution rate of the limestone but about twice the dissolution rate of dense Paleozoic dolomite.

It was concluded that differences in dissolution rate alone were only one factor in accounting for the absence of conduit development in the dolomite. It seems likely that CO_2 content and degree of saturation of infiltrating storm water also play an important role.

REFERENCES

Briggs, R.P. & Seiders, V.M. (1972). Geologic map of the Isla de Mona Quadrangle, Puerto Rico. U.S. Geological Survey Miscellaneous Geologic Map Investigations Map I-718, 1 sheet with text.

Drever, J.I. (1997). *The Geochemistry of Natural Waters*. 3rd Edition. Prentice Hall, Upper Saddle River, NJ: 436 pp.

Dreybrodt, W., Lauckner, J., Liu, Z., Svensson, U., & Buhmann, D. (1996). The kinetics of the reaction $CO_2 + H_2O \Leftrightarrow H^+ + HCO_3^-$ as one of the rate limiting steps for the dissolution of calcite in the system H_2O-CO_2-$CaCO_3$. *Geochimica et Cosmochimica Acta 60*: 3375-3381.

Frank, E.F. (1993). *Aspects of karst development and speleogenesis, Isla de Mona, Puerto Rico: An analogue for Pleistocene speleogenesis in the Bahamas*. M.S. thesis, Geology, Mississippi State University: 132 pp.

Frank, E.F., Wicks, C., Mylroie, J., Troester, J., Alexander, E.C., Jr., & Carew, J.L. (1998a). Geology of Isla de Mona, Puerto Rico. *Journal of Cave and Karst Studies 60(2)*: 69-72.

Frank, E.F., Mylroie, J., Troester, J., Alexander, E.C., Jr., & Carew, J.L. (1998b). Karst development and speleogenesis, Isla de Mona, Puerto Rico. *Journal of Cave and Karst Studies 60(2)*: 73-83.

Herman, J.S. (1982). *The dissolution kinetics of calcite, dolomite, and dolomitic rocks in the CO_2-water system*. Ph.D. thesis, Geochemistry and Mineralogy, The Pennsylvania State University: 214 pp.

Herman, J.S. & White, W.B. (1985). Dissolution kinetics of dolomite: Effects of lithology and fluid flow velocity. *Geochimica et Cosmochimica Acta 49*: 2017-2026.

Kaye, C.A. (1959). Geology of Isla Mona, Puerto Rico, and notes on the age of Mona Passage. *U.S. Geological Survey Professional Paper 317-C*: 141-178.

Levich, V.G. (1962). *Physicochemical Hydrodynamics*. Prentice Hall, Englewood Cliffs, NJ: 700 pp.

Liu, Zaihua & Dreybrodt, W. (1997). Dissolution kinetics of calcium carbonate minerals in H_2O-CO_2 solutions in turbulent flow: The role of the diffusion boundary layer and the slow reaction $H_2O + CO_2 \Leftrightarrow H^+ + HCO_3^-$. *Geochimica et Cosmochimica Acta 61*: 2879-2889.

Rauch, H.W. & White, W.B. (1970). Lithologic controls on the development of solution porosity in carbonate aquifers. *Water Resources Research 6*: 1175-1192.

Rauch, H.W. & White, W.B. (1977). Dissolution kinetics of carbonate rocks. 1. Effects of lithology on dissolution rate. *Water Resources Research 13*: 381-394.

CUEVA DE VILLA LUZ, TABASCO, MEXICO: RECONNAISSANCE STUDY OF AN ACTIVE SULFUR SPRING CAVE AND ECOSYSTEM

LOUISE D. HOSE
Department of Environmental Studies, Westminster College, Fulton, MO 65251 USA
JAMES A. PISAROWICZ
Wind Cave National Park, Hot Springs, SD 57747 USA

Cueva de Villa Luz (a.k.a. Cueva de las Sardinas) in Tabasco, Mexico, is a stream cave with over a dozen H_2S-rich springs rising from the floor. Oxidation of the H_2S in the stream results in abundant, suspended elemental sulfur in the stream, which is white and nearly opaque. Hydrogen sulfide concentrations in the cave atmosphere fluctuate rapidly and often exceed U.S. government tolerance levels. Pulses of elevated carbon monoxide and depleted oxygen levels also occasionally enter the cave.

Active speleogenesis occurs in this cave, which is forming in a small block of Lower Cretaceous limestone adjacent to a fault. Atmospheric hydrogen sulfide combines with oxygen and water to form sulfuric acid, probably through both biotic and abiotic reactions. The sulfuric acid dissolves the limestone bedrock and forms gypsum, which is readily removed by active stream flow. In addition, carbon dioxide from the reaction as well as the spring water and cave atmosphere combines with water. The resultant carbonic acid also dissolves the limestone bedrock.

A robust and diverse ecosystem thrives within the cave. Abundant, chemoautotrophic microbial colonies are ubiquitous and apparently act as the primary producers to the cave's ecosystem. Microbial veils resembling soda straw stalactites, draperies, and "u-loops" suspended from the ceiling and walls of the cave produce drops of sulfuric acid with pH values of <0.5-3.0 ±0.1. Copious macroscopic invertebrates, particularly midges and spiders, eat the microbes or the organisms that graze on the microbes. A remarkably dense population of fish, Poecilia mexicana*, fill most of the stream. The fish mostly eat bacteria and midges. Participants in an ancient, indigenous Zoque ceremony annually harvest the fish in the spring to provide food during the dry season.*

Sulfur-rich waters of hypogenic origin formed Cueva de Villa Luz (a.k.a. Cueva de la Sardina, Cueva de las Sardinas, Cueva del Azufre) two kilometers south of the pueblo of Tapijulapa, Municipio de Teapa, Tabasco, Mexico. Small springs of thermal (+3°C above regional groundwater temperature), sulfur-rich water rise through the floor of the cave, joining the four small streams that flow into the cave from cracks too small to explore. Together, they form an active, anastomozing stream that flows through and out of the cave. Hydrogen sulfide concentration in the atmosphere varies and is frequently high enough to be a significant health hazard to visitors. In addition to the cave's fascinating hydrology and atmosphere, Villa Luz has a diverse and robust biological community that appears to be largely dependent on the mineral-rich waters.

The Cueva de Villa Luz stream flows at about 80 m msl and approximately 40 m above the regional hydrologic base level, which is represented by the Amatán and Oxocotlan rivers (Fig. 1). Lush vegetation and abundant rainfall of ~550 cm (Gordon & Rosen 1962) mark the overlying tropical hills.

The cave is ~65 km from the rich oil fields near Villahermosa, which suggests a possible migration of hydrogen sulfide from petroleum reservoirs. However, the cave is also only 10 km from a Tertiary andesitic flow and 50 km from the recently erupted (1982) El Chichón volcano, which has sulfur-rich waters in its caldera (Casadevall *et al.* 1984; Taran 1998). Consequently, the source of the sulfide-rich waters has not yet been identified.

EXPLORATION AND STUDY OF THE CAVE

Although indigenous Zoque groups visited Cueva de Villa Luz for centuries, the first systematic investigation of the cave was done by biologists Gordon and Rosen (1962). They focused on the larger organisms in the cave (fish, insects, spiders, etc.).

Cavers Jim Pisarowicz and Warren Netherton (Pisarowicz 1987) were unaware of the earlier work in this area when they started exploring and mapping caves near Teapa, Tabasco. While surveying Grutas de Cócona on the outskirts of Teapa, several people told Pisarowicz and Netherton that they should go look at "Azufre," which translates to sulfur. Pisarowicz and Netherton thought at the time that they were not interested in sulfur so put off investigating "Azufre" until the last days of their trip.

In February of 1987, just two days before Netherton was to

catch a plane back to the United States, Pisarowicz and Netherton traveled to the village of Tapijulapa where they began asking about "azufre." They were directed toward a trail and told to follow it until they saw a white stream. Following the stream would lead to the cave entrance.

They found and followed the white stream until the odor of H_2S became strong and the stream emerged out of breakdown. After looking about the area, they found and descended an easier route into the cave. This entrance has been subsequently developed by the people of Tapijulapa by constructing concrete stairs into the cave.

Pisarowicz and Netherton immediately did a quick reconnaissance of the cave, wading both upstream and down. Since Netherton was to leave the next day, a discussion ensued about effectively using their time. Netherton favored beginning mapping the cave while Pisarowicz thought a photo survey of the cave should be done first. Pisarowicz's thoughts were that he had never seen similar cave features (sulfur, moonmilk-like stalactites [later dubbed snottites], ubiquitous gypsum crystals) in over 20 years of caving and that without photo documentation, few people would believe the things that they had seen. They returned to the cave with photographic equipment the next day and shot a series of pictures which were included in a presentation at the National Speleological Society convention in 1988 (Pisarowicz 1991).

In 1988, a larger expedition made a preliminary map of Cueva de Villa Luz (Pisarowicz 1988a). This expedition also began investigating the acidity of drips from snottites in the cave. Mark Minton, a caver and chemist at the University of Texas-Austin, provided Pisarowicz with several blocks of pH paper. Before entering the cave, individual pieces of pH paper were put into vials so that the acidic atmosphere of the cave would not react with all of the pH paper. During this expedition, pH of various water drops in the cave registered as low as 1.

The 1989 expedition began H_2S air sampling. A National Speleological Society grant provided a sampling pump and detector tubes to measure atmospheric H_2S. This expedition also collected elemental sulfur and gypsum samples for sulfur isotope analyses. Results indicated that the sulfur and sulfate from the cave were isotopically light and had been affected by biological processes (Spirakis & Cunningham 1992; Pisarowicz 1994).

The 1996-97 and 1998 expeditions resulted in a high-definition map of the cave (Fig. 1). The 1996-97 trip also collected, for the first time, "snottites" and wall, floor, and stream sediments for biological analysis including fixing samples for further investigation for microbes (Hose & Pisarowicz 1997a). These analyses yielded the significant finding of colonies of bacteria in extremely low pH environments. The January 1998 expedition brought a strong, interdisciplinary group of cavers, biologists, microbiologists, geologists, hydrochemists, and mineralogists to initiate detailed studies of the cave (Fig. 2).

Cave Description

Gross Passage Morphology

Total surveyed length of Cueva de Villa Luz is ~1900 m with only a few, difficult or miserable leads remaining in the cave. Total relief of the explored cave is only ~25 m. The main trend of the cave parallels the strike of the northeast trending bedrock (Fig. 3). The strike of the beds bends to a more eastward trend near the Main Entrance and the cave trend bends accordingly (Fig. 1). Passages enlarged where small, high-angle faults and joints cross them, but these minor structural features do not seem to affect the main trend of passage development. Passage upstream from the Main Entrance follows a low-angle fault.

The cave has at least 24 skylights, mostly vertical shafts with dissolution features such as natural bridges, boneyard, and rillenkarren walls. The floor is predominantly bedrock, commonly incised by the stream (Fig. 4) with only small amounts of breakdown.

Stream

About 20 small risings of thermal (28°C), sulfur-rich water entering the cave through the floor have been identified. They join four small streams that flow into the cave from cracks too small to explore, and form an active, anastomosing stream that flows through and out of the cave. pH readings taken in early January 1998 at the springs were 6.6-7.3 (±0.1) (Palmer & Palmer 1998). The cave stream had values ranged from 7.2 upstream, near the risings, to 7.4 at the resurgence (Hose & Pisarowicz 1997b). Gordon & Rosen (1962) analyzed the water and their results are shown in Table 1.

Table 1. Analysis of stream water, Cueva de Villa Luz (Gordon & Rosen, 1962)

Temperature (April 1946)	28°C throughout
Temperature (December 1955)	30°C throughout
pH	7.0 - 7.2
Chloride	1.5×10^{-2} M
Sodium	2×10^{-5} M
Potassium	3×10^{-4} M
Calcium	6×10^{-3} M
Phosphate	None detectable
Sulfate	9×10^{-3} M
Hydrogen sulfide	Faint odor throughout

The Villa Luz stream is milky and translucent to opaque, probably due to suspended elemental sulfur. Stream discharge from the main resurgence in January 1998 was at ~290 L/sec and ~270 L/sec later in the dry season, April 1998. Prolonged exposure of skin to bottom sediments, which had slightly acidic (~6.4-6.8) pH readings, under the stream with a pH of 7.2 causes a mild burning sensation. Abundant white filaments

about 2-3 cm long drift in the current. Perhaps most remarkable is the concentration of cave-adapted fish, which prompt two of the cave's alternative names, Cueva de la Sardina and Cueva de las Sardinas.

ATMOSPHERE

The odor of H₂S is apparent before entering the slightly thermal, 28°C cave. When Pisarowicz and Netherton (Pisarowicz 1987) first entered the cave in February 1987 they noted that they quickly became habituated to the "rotten egg" smell of H₂S. Fortunately, their initial reconnaissance of the cave was short as H₂S is toxic in high concentrations. In 1988, during a preliminary survey of the cave (Pisarowicz 1988ab) involving longer trips, several individuals complained about feeling ill after leaving the cave.

Starting in 1989, trips into the cave carried a Kitagawa pump to draw air samples through H₂S length-of-stain detector tubes (Kitagawa type SA and SB). Nine trips into the cave in 1989 during February and March, three trips in December 1996, and six trips in January 1997 took a total of 82 air samples for analysis at eight different locations in the cave. These results are summarized in Table 2.

In general, the atmospheric H₂S levels were higher further back into the cave, with the highest levels in the Sala Grande-Bat Room area. In areas near skylights (Main Entrance Room and Sorpresa de Jaime), H₂S concentrations were generally lower. This is presumably due to mixing of cave and outside air. Also notable is that H₂S measurements in the slightly higher, dry Fresh Air passages were the lowest throughout the cave.

Recent trips into Cueva de Villa Luz have used H₂S/SO₂ filtering respirators. When exploration of Villa Luz began in 1987, the threshold limit value (TLV) for H₂S established by the American Conference of Governmental Industrial Hygienists was 10 PPM (NIOSH 1994). Recently the Environmental Protection Agency has established a "no tolerance" limit for H₂S exposure.

We recently received an Enmet Quadrant Four-Gas Monitor (H₂S, O₂, CO, and flammable gases). In April 1998, the monitor recorded a carbon monoxide (CO) level of 48 PPM at stream level in Snot Heaven. Hydrogen sulfide concentra-

Table 2. Analyses of air samples taken in Cueva de Villa Luz. SD - standard deviation on data; N - number of samples at site; Range - concentrations in parts per million as determined by a Kitagawa pump drawing air samples through H₂S length-of-stain detector tubes (Kitagawa type SA and SB).

Location	Mean	SD	N	Range
Main Entrance Room	15.67	7.50	18	6-30
Big Room by Cat Box	19.22	5.81	9	10-27
End of Zoo-downstream	5.67	3.65	9	1-12
Sala Grande-Bat Room	40.00	10.72	10	25-55
Sala Grande	18.22	6.11	9	8-25
Fresh Air area	1.00	1.05	9	0-3
Entrance-Skylight	11.11	6.01	10	3-18
Zoo	9.89	4.38	9	3-16

tions at the same time measured up to 152 PPM and oxygen (O₂) dropped to 9.6% (Taylor 1999). The event lasted less than 30 minutes (the area was evacuated so the exact timing is unknown). We experienced a similar "burst" in the upstream part of The Other Buzzing Passage in January 1999 (CO at 85 PPM, H₂S at 120 PPM, and O₂ at 9.6%). The Other Buzzing Passage consistently registered the highest H₂S levels, except for occasional outgassing events elsewhere. Upstream Cueva de Villa Luz should only be entered by individuals prepared to deal with such conditions.

LIFE IN THE CAVE

Life is abundant in the cave including plentiful bats and invertebrates. Various slimes and pastes coat the walls and floors throughout the cave. Unique to Villa Luz are growths of white, mucous-like soda straws, curtains, and "u-loops" up to 50 cm long suspended from walls and ceilings (Fig. 5). Original explorers referred to these deposits as "snottites" (Pisarowicz 1988c). Although they hang throughout the cave, they are most concentrated near the springs, particularly in Snot Heaven. Water drops from these growths had pHs of 0.0-3.0 (±0.1). The abundance of snottites was markedly greater in January 1997 than January 1998, a drier year, and even fewer hung in the cave in April 1998, further into the dry season. Atmospheric H₂S levels also declined over the three trips.

These phlegm-like materials were dyed with diamidinophenylindole (DAPI) stain, which causes material with DNA to fluoresce, and then examined under a 400x magnification with ultraviolet light. Inspection revealed that the "snottites" are communities of microbes similar to microbial mats commonly associated with sulfur-rich surface springs, but these colonies are suspended vertically. Mites, midges, worms, and various other invertebrates are commonly seen on these microbial "veils" despite the very low-pH environment (Fig. 6).

A green, slimy coating covers bedrock and breakdown immediately above water level throughout much of the cave, even in places beyond apparent visible light (The Other Buzzing Passage). Small, flying insects [probably the midge larvae] gather on these growths, apparently to graze. Spherical microbes larger than cyanobacteria mostly make up the green material.

A diverse variety of other organic and partially organic slimes coat the walls and floors. Slimy, brown, anastomosing and splotchy biovermiculations commonly coat the limestone walls. Microscopic examination revealed them as colonies of bacteria and fungi (Fig. 7). Many biovermiculation colonies were notably desiccated and represented by faint discolorations of the walls during the dry April 1998 trip. White, red, and black slimes are also abundant throughout the cave.

Figure 1 (next pages). Map of Cueva de Villa Luz, including location. Map by Bob Richards and L.D. Hose.

CUEVA DE VILLA LUZ

Tabasco, Mexico

MAIN PASSAGE
Profile View

SULFUR SPRING

SNOT HEAVEN

THE OTHER BUZZING PASSAGE

YELLOW ROSES ROOM

The Zoo
Profile View

BAT ROOM

Fault

CASA DE LOS MURCIELOGOS

Chibitil

SALON DE LOS MURCIELOGOS

SALA GRANDE

Fresh Air Section

Itchy Passage

THE ZOO

Midway Spring

THE ZOO PASSAGE - Profile

SNOT HEAVEN

SALA GRANDE

SALON DE LOS MURCIELOGOS

0
10 m
20 m
30 m
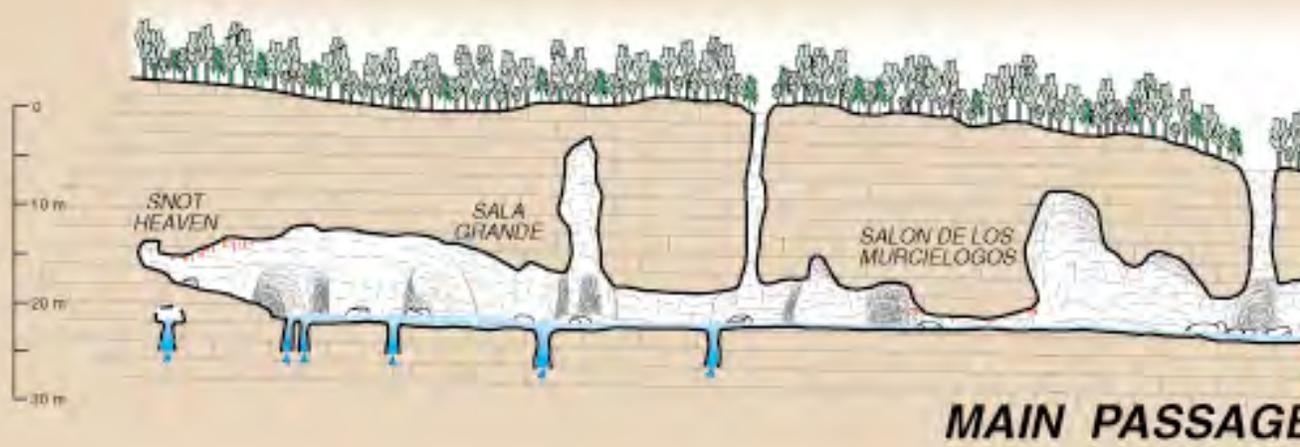
MAIN PASSAGE
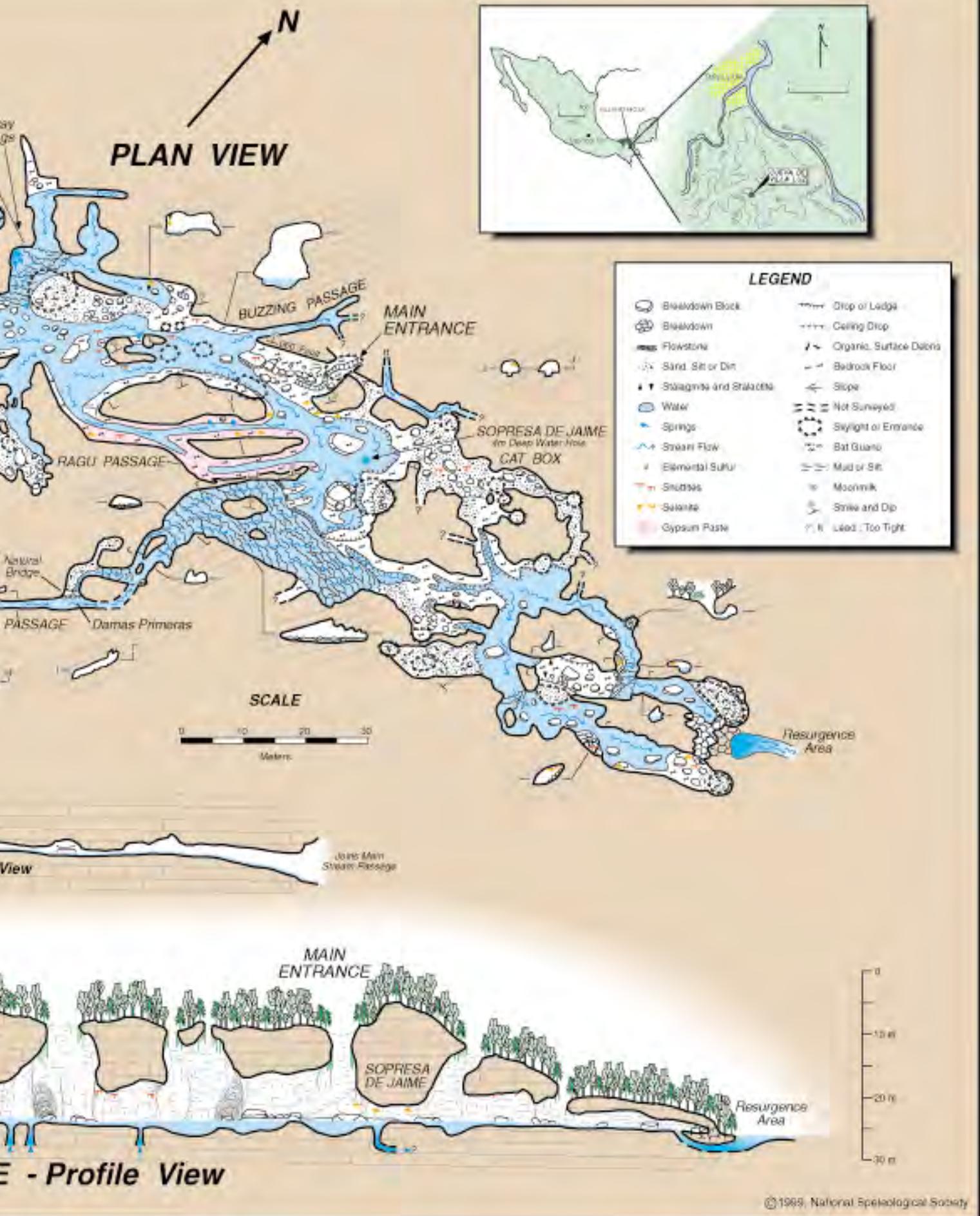
Secondary deposits

Calcite speleothems are sparse in Villa Luz. Travertine deposits form where spring waters mix with the cave stream in Snot Heaven and Midway Springs. Other poorly developed flowstone deposits are forming near Casa de los Murciélagos, at the northeast end of the Zoo, and at the entrance to The Other Buzzing Passage. A few, heavily corroded, stalactites and draperies hang from the walls of the main passage just upstream from the Main Entrance. Modest displays of stalactites and stalagmites occur in the fossil, Fresh Air section.

The most abundant speleothems in Villa Luz are splays of selenite crystals, common on the subaerial bedrock walls throughout the stream passages. Clusters and aggregates of selenite crystals are commonly located on the lower parts of ceiling pendants and on downward-facing ledges. The typically 2-4 cm long individual crystals are commonly associated with clusters of finely crystalline elemental sulfur and the microbial veils (snottites) (Fig 5). A small display of boxwork on the west side of Sala Grande was immediately adjacent to gypsum splays and elemental sulfur crystals.

White moonmilk and black, brown, orange, green, and red slimy coatings commonly cover the walls. A pasty covering of the floor in much of the cave, under 400x magnification, is mostly microcrystalline gypsum. pH of the gypsum paste is typically 1.0-3.0. Prolonged exposure to the gypsum paste (under a knee pad) resulted in a third-degree burn to one visitor.

Local usage of the cave

For centuries, the local Zoque (a.k.a. Soque) people performed a religious ceremony, La Ceremonia de la Pesca, near and in the cave. The ritual, carried out at the end of the dry season, was believed to ensure a fertile summer growing season and provided a rich source of protein until the new crops matured. It was apparently prompted by an interpretation that the cave's unique fish population was a special gift from the Zoque gods, who inhabit the underground. Dressed in indigenous costumes, Zoque elders offered prayers and requested permission to enter the cave and harvest fish. When the "grandfather" and "grandmother" guardians of the cave gave permission, the Zoque went about 100 m upstream from the main entrance where they emptied packets of crushed roots of a barbasco vine and lime into the stream. The mixture placed in water, a traditional fishing technique in Central America, reportedly ties up oxygen and forces the anoxic fish to the surface and concentrated along the edges of the stream. The Zoque then easily scooped fish up in baskets. The fish were dried and helped nourish the people through the following months. The formal ceremony was discontinued in the mid-1940s as the indigenous religion and language in the area was lost to European culture.

In 1987, a local man named José Vasquez motivated some of the Tapijulapa men to re-enact the ritual. A troupe of mostly adolescents from Tapijulapa now perform the ceremony every spring with an adult leader speaking modern Maya (Fig. 8). Concern about the possible negative impact on the fish population has prompted a more conservative approach resulting in just a token harvest.

Geology and hydrology

Cueva de Villa Luz is the only known cave within this small block of massive, micritic Lower Cretaceous limestone in a northwest-trending anticline truncated and uplifted on the south by an east-northeast-trending normal fault (INEGI 1989). The northeast-trending cave, as well as the surface and sub-surface springs, appears formed in the north-northwest-dipping strata along the downthrown side of this fault. At least nine other smaller sulfur-rich springs rise along the fault trend with similar temperature and pH values to the springs in the cave. Visible gas bubbles accompany only three of the surface springs and two of the subsurface (both in The Other Buzzing Passage) springs. Perhaps the other risings have already degassed in a previous chamber before entering the explorable cave or reaching the surface. The gas bubbles are suspected to be carbon dioxide (CO_2), but this suspicion is unconfirmed.

Other detached blocks of similar limestone contain caves nearby. Water rising into the swimming pools at El Azufre, a sulfur spring resort 27 km to the west-northwest, comes from a phreatic cave system. The temperature and chemistry of the waters are markedly similar to the cave water in Villa Luz. We are unaware of any attempts to explore the El Azufre caves. About 7km east of El Azufre, the commercial Grutas de Cócona appears to have mostly formed from hypogenic waters in the past. In a separate block of limestone only about 1 km east of Villa Luz, Grutas de Cuesta Chica appears to also represent a paleo-hypogenic cave.

Speleogenesis

Cueva de Villa Luz is clearly forming from rising, sulfur-rich water with very little meteoric input. The cave looks to have originally formed while the bedrock was saturated with the rising, sulfur-rich water. We interpret the skylights as former vents for rising spring waters similar to the springs at El Azufre.

Downcutting by the nearby river and the accompanying drop in the local groundwater base level mostly drained the cave. The rising waters now emerge through the floor of the cave and form a stream that flows through the air-filled chambers. The rising water is slightly acidic and, combined with the highly acidic drip and condensate waters in the cave, probably causes the incised channels in the floor (Figure 4) and rillenkarren-lined stream shorelines.

As the water enters the oxygenated, sub-aerial cave environment, H_2S combines with O_2 to form elemental sulfur:
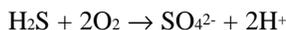
$$2\ H_2S + O_2 \rightarrow 2S° + 2H_2O$$
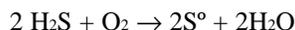
Microbes may sometimes be involved in this reaction but this initial oxidation reaction can also proceed rapidly by abiotic processes.

Microbes, particularly in the microbial veils, further oxidize the sulfur to form sulfuric acid in the following reactions:

$$2S^o + 3O_2 + 2H_2O \rightarrow 2SO_4^{2-} + 4H^+$$

and

$$H_2S + 2O_2 \rightarrow SO_4^{2-} + 2H^+$$

The acid dissolves calcite in the limestone and the freed calcium ions then combine with the sulfate ions to form gypsum:

$$CaCO_3 + 2H^+ \rightarrow Ca^{2+} + H_2O + CO_2$$

$$Ca^{2+} + SO_4^{2-} + 2H_2O \rightarrow CaSO_4 \cdot 2H_2O$$

Other biotic and abiotic reactions may achieve the same end result (Spirakis & Cunningham 1992). In addition, carbon dioxide and water undoubtedly combine to form carbonic acid that assists in the dissolution of the cave. Carbon dioxide comes from the atmosphere and rises in the hypogenic water as well as from the above reaction.

The current input of H_2S and the aggressive microbial communities promote active speleogenesis. Surely, passages are enlarging and, given the near-surface setting of the cave, Cueva de Villa Luz in its current vadose stage must be an ephemeral feature.

ECOSYSTEM OF THE CAVE

Preliminary investigations suggest a robust ecosystem in the cave that derives most its energy from chemoautotrophic processes. Downstream passages also receive energy input from bat guano and surface debris washing into the skylights.

Microbial communities, such as the microbial veils that oxidize reduced forms of sulfur create a base of the cave's food web. Sulfur-reducing microbes continue utilizing energy from the sulfur cycle. Fungi and other microbes derive further energy from the chemoautotrophs.

An extremely dense population of midges, *Tendipes fuvipilus* Rempel (Gordon & Rosen 1962; Langecker *et al.* 1996), is ubiquitous in the stream passages, particularly clustering on the green slime immediately above the stream. The midges, or perhaps their larvae, probably graze on the bacteria. Abundant spiders, beetles, mites, crickets, and other invertebrates presumably feed on either the microbes, midges, or each other.

The fish, *Poecilia mexicana* Steindachner 1863 (Gordon & Rosen 1962; Langecker *et al.* 1996), are the most striking inhabitants of the cave. Stomach analyses (Langecker *et al.* 1996) revealed a diet of dominantly bacterial filaments and midge larvae. Some downstream populations derive a minor portion of their diet from bat guano. Diana Northup and Kathleen Lavoie (personal communication, 1998) observed a diving hemipteran capture and devour a fish. Humans are the only other documented predators of the fish. A copious food supply and scarcity of natural predators facilitate the abundant fish population.

Several other vertebrates inhabit or frequent the cave. Several species of bats reside in the cave including four species of the Phyllostomid family (Gordon & Rosen 1962), a freetail, and a vampire species. Some of the bats seem to be extraordinarily active during the day. Obvious questions for future research include whether they feed on the dense midge population in the cave and how they cope with the high toxic gas levels. (It is notable that several dead and dying bats hung from the walls in the stream passage during most visits). Sightings of eel, an accidental(?) turtle and abundant footprints of a probable tepeizcuinte (*Agouti paca*) make up the other evidence of vertebrates observed in the cave.

DISCUSSION

Cueva de Villa Luz is a striking example of sulfur-related speleogenesis and a chemoautotrophic ecosystem. Although not unique, its apparently robust ecosystem, high-energy environment, and easy access suggest that the cave will prove an excellent site for studies in both fields. The historic, and probable prehistoric, indigenous ceremonial use of the cave promises another intriguing field of investigation. We hope that the current, excellent relations with the local residents and officials will continue to facilitate work at the cave.

Other current studies at the cave include preliminary investigations into the hydrochemistry and related topics by Art and Peggy Palmer (SUNY-Oneonta), microbial biology by Diana Northup (University of New Mexico), Penny Boston (Complex Systems Research, Inc.), and Kathy Lavoie (SUNY-Plattsburg), invertebrate biology studies by José Palacios-Vargas (Universidad Nacional Autonoma de Mexico) and Carlos Blanco-Montero (Rohm and Haas Company, Agricultural Chemicals North America), sulfur mineralogy by Harvey DuChene (NSS), and a two-plus year aquarium study of the fish by Jakob Parzefall and colleagues at the University of Hamburg. With so much interest in the cave, it seems imperative that our next course of investigation be to improve understanding of the cave atmosphere, particularly the nature of the degassing events, and to improve safety procedures.

ACKNOWLEDGMENTS
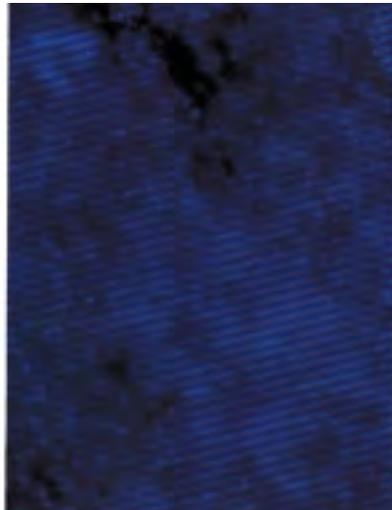
Figure 2 (top left). January 1998 group picture. Photo by Carl Snyder.

Figure 3 (center left). Looking upstream in Sala Grande. Note the stream is parallel to the strike of the beds in the ceiling over the caver. Photo by J.A. Pisarowicz.

Figure 4 (top right). Incised stream channel in downstream portion of cave. Photo by J.A. Pisarowicz.

Figure 5 (bottom left). Snottites in Snot Heaven. Photo by L.D. Hose.

Figure 6 (bottom center). Photomicrograph of a DAPI-stained snottite—400x. Photo by L.D. Hose.

Figure 7 (bottom right). Photomicrograph of DAPI-stained bacterial and fungal colonies in graphic, brown slime deposits (biovermiculations)—400x. Photo by L.D. Hose.

Figure 8 (center right). Re-enactment of La Ceremonia de la Pesca at Cueva de Villa Luz. Photo by L.D. Hose.

REFERENCES

Casadevall, T.J., Cruz-Reyna, Servando de la, Rose, W.I., Bagley, S., Finnegan, D.L., & Zoller, W.H. (1984). Crater lake and post-eruption hydrothermal activity, El Chichón Volcano, Mexico: *Journal of Volcanology and Geothermal Research*, *23*:169-191.

Gordon, M.S. & Rosen, D.E. (1962). A cavernicolous form of the Poeciliid fish *Poecilia sphenops* from Tabasco, Mexico: *Copeia*, n. 2: 360 - 368.

Hose, L.D., & Pisarowicz, J.A. (1997a). Exploration and mapping of Cueva de Villa Luz (Cueva de la Sardina), Tabasco, Mexico. *Journal of Cave and Karst Studies, 59*(3): 173.

Hose, L.D., & Pisarowicz, J.A. (1997b). Geologic setting of Cueva de Villa Luz–A reconnaissance study of an active sulfur spring cave. *Journal of Cave and Karst Studies, 59*(3): 171.

INEGI (1989). *Carta Geologica* (geologic map) - *Villahermosa* (scale 1:1,000,000).

Langecker, T.G., Wilkens, H., & Parzefall, J., (1996). Studies on the trophic structure of an energy-rich Mexican cave (Cueva de las Sardinas) containing sulfurous water: *Mémoires de Biospéologie*, Tome XXIII: 121-125.

NIOSH (1994). *NIOSH Pocket Guide to Chemical Hazard*. National Institute for Occupational Safety and Health, Centers for Disease Control and Prevention: 171-172.

Palmer, A.N. & Palmer, M.V. (1998). Geochemistry of Cueva de Villa Luz, Mexico: An active H_2S cave. *Journal of Cave and Karst Studies, 60*(3): 88.

Pisarowicz, J.A. (1987). Caving in Tabasco. *Association for Mexican Cave Studies Activities Newsletter 16*: 30-37.

Pisarowicz, J.A. (1988a). Revenge of Chac: 1988 in Tabasco. *Association of Mexican Cave Studies Activities Newsletter 17*: 129-138.

Pisarowicz, J.A. (1988b). Southern Mexican caving-Tabasco 1988. *Rocky Mountain Caving 5*(3): 25-28.

Pisarowicz, J.A. (1988c). Field notes for the 1988 Caves of Tabasco Project (unpublished).

Pisarowicz, J.A. (1991). Caving in Tabasco, Mexico. *National Speleological Society Bulletin 53*(1): 29.

Pisarowicz, J.A. (1994). Cueva de Villa Luz-An active case of H_2S speleogenesis. In Sasowsky, I.D. & Palmer, M.V. (eds.) *Breakthroughs in Karst Geomicrobiology and Redox Geochemistry*. Special Publication 1, Karst Waters Institute, Charlestown, WV: 60-62.

Spirakis, C.S. & Cunningham, K.I. (1992). Genesis of sulfur deposits in Lechuguilla Cave, Carlsbad Caverns National Park, New Mexico. In Wessel, G. and Wimberly, B. (eds.) *Native Sulfur-Developments in Geology and Exploration: American Institute of Mining Engineers (AIME) Special Volume*. Chapter 11: 139-145.

Taran, Y., Fischer, T.P., Pokrovsky, B., Sano, Y., Aurora-Armienta, M., & Macias, J.L. (1998) Geochemistry of the volcano-hydrothermal system of El Chichón volcano, Chiapas, Mexico: *Bulletin of Volcanology, 59*: 436-449.

Taylor, M.J. (1999) *Dark Life: Martian Nanobacteria, Rock-Eating Cave Bugs and Other Extreme Organisms of Inner Earth and Outer Space*. Scribner: 287 pp.

ISOTOPIC STRATIGRAPHY OF A LAST INTERGLACIAL STALAGMITE FROM NORTHWESTERN ROMANIA: CORRELATION WITH THE DEEP-SEA RECORD AND NORTHERN-LATITUDE SPELEOTHEM

STEIN-ERIK LAURITZEN

Department of Geology, University of Bergen, Allégaten 41, N-5007 Bergen, NORWAY (stein.lauritzen@geol.uib.no)

BOGDAN PETRONIU ONAC

Department of Mineralogy, University of Cluj, Kogalniceanu 1, 3400 Cluj, ROMANIA (bonac@bioge.ubbcluj.ro), Speleological Institute (Emil Racovita), Clinicilor 5, Cluj, ROMANIA

LFG-2, a 39.5 cm tall stalagmite from northwestern Romania, has been dated by U-series α-spectro-metric dating, and analyzed for stable isotope variations (δ¹⁸O, δ¹³C) along its growth axis. The sample grew all the way through oxygen isotope stage 5(a-e), and perhaps for some time into stage 4. In spite of a rather low uranium content and therefore imprecise chronology, the sample provides an interesting stable isotope record with high temporal resolution that correlates favorably with other speleothems and with the deep-sea record. Termination II is well defined in the record as a rapid shift from light (cold) to heavier (warm) δ¹⁸O values, when C3 vegetation seemed to dominate. The δ¹³C in a slow growth zone, corresponding to oxygen isotope stage 5d, as well after the stage 5/4 transition, suggests that C4 plants possibly dominated the surface environment. The δ¹⁸O record also correlate quite well with the α-dated FM-2 record from northern Norway.

Speleothems are important paleoclimatic and chronological archives because they are continental deposits and well-suited for uranium series disequilibrium dating. Besides the dating potential by U-series methods (Schwarcz 1986), which yield data about climate-controlled growth range (Gascoyne *et al*. 1983) and growth frequency (Gordon *et al*. 1989; Baker *et al*. 1993b; Lauritzen 1993b; Onac & Lauritzen 1996), speleothems also carry a vast range of paleoclimatic proxies, like stable isotopes (Lauritzen & Lundbergdi 1998; Rowe *et al*. 1998), growth laminae (Baker *et al*. 1993a; Shopov *et al*. 1994; Genty & Quinif 1996), natural organic matter (NOM) Lauritzen *et al*. 1986; Ramseyer *et al*. 1997), microfossils, such as pollen (Bastin 1978; Lauritzen *et al*. 1990). Finally, speleothems preserve paleomagnetic signals (Latham *et al*. 1979, 1989; Perkins & Maher l993), which can be accurately dated.

Karst areas are regionally widespread, and speleothems can yield consistent paleoclimatic proxy data from large geographic areas. Therefore, the Speleothem Pole-Equator-Pole Project (SPEP) has been launched under the PEP activities (Lauritzen 1998). In the SPEP-III project, which aims at comparing speleothem data along a north-south transect from Spitzbergen and Norway (Lauritzen 1995; Lauritzen & Lundberg 1998) to South Africa (Holmgren *et al*. 1994, 1998), Romania, situated well beyond the limits of the Scandinavian glaciations, plays an important role with its continental climate. Our results so far have revealed that time-dependent speleothem growth frequency is less sensitive to climatic change at this location than at higher latitude areas, such as the British Isles and North Norway (Baker *et al*. 1993b; Lauritzen 1993b; Lauritzen *et al*.

1996; Onac & Lauritzen 1996). In this paper we present the results of detailed chronostratigraphic studies of a *single* speleothem, the LFG-2 stalagmite from Lithophagus Cave in northwestern Romania.

MATERIAL AND METHODS

THE LITHOPHAGUS CAVE

The Lithophagus Cave is located in the Middle Basin of Iada Valley, within the eastemmost part of the Pădurea Craiului Massif (Apuseni Mountains, Transylvania, Fig. 1). More than 250 caves and potholes are distributed on 5 different karstification levels with a vertical extent of 350 m (Tamas & Vremir, 1997). The most important cavities in this region were discovered during intensive mining and hydroelectric tunneling.

The cave, which is formed in Upper Jurassic (Tithonian) limestone, opens on the southern side of the valley at a relative altitude of 55 m (545 m msl) (Vremir 1994). It consists of several isolated phreatic and vadose galleries and chambers totaling 620 m in length, interrupted in a few places by mining galleries (collapses, storage spaces, etc). The name, Lithophagus

Figure 1.
Key map of Romania with the investigated area.

Figure 2.
Plan map of Nelus cave in the Lithophagus Cave system (a), with inset (b) showing passage cross-section with sample site.

The stalagmite (LFG-2) is 39.5 cm high. The lowest samples for U-series dating and isotopic analysis were extracted from 1.5 cm above the base of the speleothem (Fig. 3).

The outside part of the stalagmite is randomly covered by millimeter-sized botryoidal or coral-like calcite speleothems that were presumably formed by splashing or rapidly dripping water rebounding from the gravel floor or from neighboring speleothems.
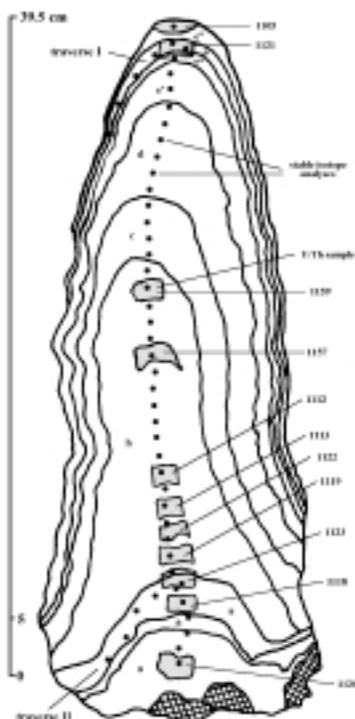
The speleothem was cast in plaster for stabilization and cut into several 1 cm thick slices parallel with the growth axis. Each slice was briefly etched in dilute HCl, washed, ground and polished. The cross-section (Fig. 3) exhibits several growth zones visible to the naked eye. The most important ones were analyzed microscopically on six thin sections. This revealed that boundaries between growth layers represent 1) linear concentration of gas or liquid inclusions, 2) impurity-rich layers, 3) changes of the calcite crystal habit during growth, and 4) layers of micritic calcite crystals.

Thus, we have divided the sample into 5 morphological zones labeled a, b, c, d and e in Fig. 3:

Zone «a» (0 to 75 mm): Very fine laminae made up of length-slow calcite (Folk & Assereto 1976), outlined by abundant gas/liquid inclusions;

Zones «b» & «c» (75 mm to 290 mm): Translucent to clear calcite laminae, slightly similar in fabric to zone «a» but with fewer inclusions. Most of the growth-layering within zones «b» and «c» is defined by abrupt changes in either inclusion density or crystal morphology. The «b/c» boundary is given by a clear brown impurity layer at 265 mm from base. The length-slow calcite crystals are replaced by length-fast crystals as they approach the boundary to zone «d»;

Zone «d» (290 mm to 350 mm): This zone consists of ordinary length-fast calcite crystals that build clear columnar crystals (palisade fabric) (Kendall & Broughton 1978). It is difficult to estimate the width of the crystals as they are nearly parallel to each other and show semicomposite to weakly undulose extinction. Just above the lower boundary, the *c-axes* of the calcite crystals tend to lie subhorizontally (at an angle between 40° to 85° from the vertical), but further up, due to geometrical selection (Grigor'ev 1965; Dickson 1993), the *c axis* becomes perpendicular to the growth surface. The calcite crystals in this zone are transparent to translucent and have very few inclusions;

Zone «e» (350 mm to 395 mm): The upper part of the stalagmite consists of two sub-zones of white opaque calcite laminae, very porous and full of inclusions (Fig. 3, «e1») and two other sub-zones of clear to translucent layers made up of columnar calcite crystals (Fig. 3, «e2»).

("stone eater"), comes from the fact that more than 7000 m³ of barren gangue were consumed or "eaten" by the cave. The cave has no natural entrances, and it is likely that it has stayed as a closed cavity for a very long time in the past.

The LFG-2 stalagmite was collected from a 30 m long side passage in Nelus Cave (part of the Lithophagus Cave system), just below the mining gallery (Fig. 2a) (Onac 1996). The speleothem grew on top of a 3 to 4 cm thick flowstone that itself covered collapsed limestone boulders (Fig. 2b).

Figure 3.
Longitudinal section of stalagmite sample LFG2 with location stable isotopes (black spots), $^{230}Th/^{234}U$ dating (grey boxes), and (a-e). a: fine laminae of length-slow calcite; b & c: translucent to numerous abrupt changes; d: length-fast, palisade calcite; e: a white calcite (e'), and clear columnar calcite (e").

Length-slow calcite crystals began their growth on a disconformity surface, and due to variable flow rate (i.e local 'wetness' in the cave), the calcite crystals composing zone «a» are of unequal size and form a porous fabric. Normal length-

fast calcite that prevails in zones «b», «c» and «d» suggests a wet (local) environment with no significant changes in the chemistry of the dripwater (which would otherwise have precipitated different types of calcite crystals), although there are intervals when calcite precipitation rate was attenuated or even ceased. For instance, changes in the $\delta^{18}O$ values below and above the «b/c» zone boundary (295 mm from base), where a layer of brown calcite was precipitated, would indicate such an event marked by changes in calcite crystal fabric from length-slow (just above this brown layer) to length-fast for the rest of the zone. Therefore, zone «b» probably experienced slow growth under mostly wet conditions. In zone «c», the precipitation commenced at a slow rate under wet conditions and increased as it approached the boundary with zone «d». Zone «d» is made up of length-fast calcite crystals which developed under wet conditions, but the crystallization rate was rather slow. Within zone «e», there are 2 sub-zones («e1») that indicate mostly dry and fast growth (very porous material) while the other 2 sub-zones («e2») are characteristic for slow growth under non-drying conditions.

URANIUM-SERIES DATING

Uranium-series disequilibrium dating can be performed on speleothems provided sufficient U is present (> 0.02 ppm) and that the system was initially free from non-authigenic ^{230}Th, as monitored with the $^{230}Th/^{232}Th$ index (Latham & Schwarcz 1992). Fourteen subsamples (10-15 mm thick, 10-60 g) were removed at regular stratigraphic levels for U-series dating, of which 11 contained sufficient U for dating (Fig. 3). The samples were digested in excess nitric acid, spiked ($^{228}Th/^{232}U$) and equilibrated by H_2O_2 oxidation and boiling for several hours. U and Th were pre-concentrated by scavenger precipitation on ferric hydroxide. Iron was then removed by ether extraction in 9M hydrochloric acid, and U and Th separated by ion exchange chromatography on Dowex 1 resin. The purified, carrier-free fractions of U and Th were then electroplated onto stainless steel disks and counted for alpha particle activity *in vacuo* on an Ortec Octéte unit with silicon surface barrier detectors for 2-4 days. Each spectrum was corrected for background and delay since chemical separation and processed by tailored software (Lauritzen 1993a). All dates were performed at the Uranium-Series Geochronology Laboratory at the Department of Geology, University of Bergen.

STABLE ISOTOPES IN SPELEOTHEMS

The oxygen isotopic composition of speleothem carbonate, $\delta^{18}O_c$, precipitated in isotopic equilibrium with the dripwater (Hendy 1971; Gascoyne 1992), may be expressed as the *Speleothem Delta Function* (Lauritzen 1995,1996):

$$\delta^{18}O_c = e^{\left[\frac{a}{T}-b\right]}\left[F(T,t,g)+10^3\right]-10^3 \qquad \text{[1]}$$

where T is absolute temperature, t is time and g is geographi-

cal position of the site. Equation **[1]** has two terms. The first (exponential) term with constants a and b represents the *thermodynamic fractionation* factor ($\alpha_{c\text{-}w}$) between calcite and water (later called $\mathbf{T_{fr}}$). The second term contains the *dripwater function*, F(T,t,g). Here, the T-dependence relates to the atmospheric precipitation at a site, while the t- and g-dependence represent the transport history of rain and various properties of the weather system producing the rainfall. (It is also assumed that the cave temperature equals the annual mean of the surface temperature). This sensitivity is further modulated by storage and mixing of the percolation water above the cave. There might also be a seasonal interception bias in aquifer recharge above the cave, dependent on the fraction of precipitation that actually enters the epikarst (Lauritzen 1995).

The components $\mathbf{T_{fr}}$ and F(T,t,g) have different temperature sensitivities. $\mathbf{T_{fr}}$ always has a negative response to temperature (i.e. shifts to heavier $\delta^{18}O_c$ values imply decreasing cave temperature), whilst F(T,t,g) may respond either positively or negatively, depending on regional meteorology, like rain-out effects. Consequently, the temperature response of speleothem carbonate is entirely dependent on the relative magnitude of $\mathbf{T_{fr}}$ and F(T,t,g). The *temperature response* (μ) of **[1]** is, in mathematical terms, its T-derivative (Lauritzen, 1995) defined as:

$$\mu = \frac{\partial}{\partial T}\left(\delta^{18}O_c\right) \qquad \text{[2]}$$

which can, in principle, be negative, zero or positive. This can be further discussed with respect to the relative magnitudes of the T-responses of its components, $\mathbf{T_{fr}}$ and F(T,t,g):

1. when $\mu > 0$, the F(T,t,g) response is positive and large enough to dominate over $\mathbf{T_{fr}}$.
2. when $\mu = 0$, the $\mathbf{T_{fr}}$ and F(T,t,g) responses cancel and
3. when $\mu < 0$, the F(T,t,g) response is negative or positive (if positive, it has a smaller absolute effect than $\mathbf{T_{fr}}$).

In the cases of $\mu > 0$ or $\mu << 0$ variations in $\delta^{18}O_w$ of the precipitation dominate. The temperature sensitivity and therefore the interpretation of speleothem $\delta^{18}O_c$ is by no means straightforward and often ambiguous.

However, this ambiguity may be overcome in several ways that either aim at estimating F(T,t,g), or the sign of μ:

First, F(T,t,g) at a given point in time and space can be estimated from fluid inclusions within the calcite, which are actual samples of the original dripwater at the time of precipitation. Here, $\delta^{18}O_w = F(T,t,g)$ must be estimated from δ^2H_w, via the so-called 'meteoric water line', or its local equivalent (Craig 1961; Gat 1980):

$$\delta^{18}O_w = \tfrac{1}{8}\delta^2H_w - \tfrac{10}{8} \qquad \text{[3]}$$

Then, temperature can be calculated directly from the thermodynamic term of [1] (Schwarcz & Yonge 1983; Rowe *et al.* 1998).

Second, independent evaluation of paleowater $\delta^{18}O_w$ may be extracted from other sources, such as fossil aquifers (Talma & Vogel 1992).

Third, given that some temperature estimates exist together with calcite $\delta^{18}O_c$ values for both present and past conditions, like today and well-defined historic thermal events, (e.g. the Little Ice Age), the dripwater function may be calibrated by using a simple linear relationship between temperature and isotopic composition (Dansgaard 1964). Assuming that the values of the two constants are valid for timespans beyond the calibration range, the $\delta^{18}O_c$ record may then be transformed to absolute temperature (Lauritzen 1996; Lauritzen & Lundberg 1998).

Finally, by comparing trends in the $\delta^{18}O_c$ time-series with present-day $\delta^{18}O_c$ of stalactite tips (i.e. Holocene, non-glacial conditions) and known climatic changes in the past, the sign of (m) may be judged and assumed valid for the rest of the time-series (Schwarcz 1986).

At present, the carbon isotope signal in speleothem is much more difficult to interpret than for oxygen, because shifts in $\delta^{13}C$ values are dependent on several variables that cannot be measured. Variations of $\delta^{13}C$ in speleothem carbonate are determined by the metabolic processes that control the composition of the soil CO_2, the drip rate of the cave water, the amount of bedrock carbonate that goes into solution, and the rate of outgassing and precipitation (Schwarcz 1986; Dulinski & Rozanski 1990). In regions where a change between C3 and C4 vegetation is possible, speleothem carbonate with $\delta^{13}C$ values of about -13‰(PDB) reflects an environment dominated by C3-vegetation, whereas carbonates with $\delta^{13}C$ values of approximately +1.2‰ reflect a pure C4-biomass. C4 grasses are adapted to drought stress and grow preferentially where temperatures in the growing season are above 22.5°C and minimum temperatures never go below 8°C, as for example in South Africa and Israel (Talma *et al.* 1974; Holmgren *et al.* 1995; Bar-Matthews & Ayalon 1997).

At northern latitudes, C4 vegetation is lacking, so that variations in $\delta^{13}C$ may be interpreted as changes in soil productivity and amount of bedrock interaction, which in part is governed by temperature. Northwest Romania does not have any present-day C4 vegetation, although the loess steppes that expanded in central Europe (e.g. Hungary) during glacial maxima, might have had a proportion of C4 grasses. The only Romanian evidence for climatic changes during the last interglacial was presented by Diaconeasa *et al.* (1976) showing a mixed C3 and C4-type vegetation community from the central part of the Transylvanian basin. More detailed proxy records are available from the Middle Danubian Basin (Hungary), 100 to 200 km west of our cave. Pollen analysis data indicated that during the last interglacial short periods of climatic changes can be recognized as the C3 vegetation was replaced by steppe communities dominated by C4-type vegetation (Urban 1984;

Jarai-Komlodi 1991). Furthermore, several loess cores from the central and eastern parts of Hungary show evident changes from forest soils to forest-steppe and steppe soils during isotope stage 5 (Pécsi 1993). From the vegetational point of view this means a shift from C3 to C4-type plants, a fact that agrees well with the rest of Central-Eastern Europe (Willis 1994).

Often, $\delta^{13}C$ and $\delta^{18}O$ display some covariation along the growth axis of a speleothem, suggesting that they both depend of the same external parameter, i.e. temperature. Shopov *et al.* (1997) suggested one possible explanation for this kind of effect but it is too elaborate to be included here.

Samples for stable isotopes were taken (100-200 μg each) at 10 mm intervals along the growth axis by means of a dentist's drill (Fig. 3). Also, two traverses for testing the Hendy (1971) criteria (*vide infra*) were made along growth layers at 50 mm and 375 mm above basis datum (Fig. 3). Yet another four analyses were made on crystal growth surfaces of stalactite tips sampled in the cave ceiling directly above LFG 2, in order to obtain values of recent calcite. All samples were analyzed for oxygen and carbon isotopes in CO_2 expelled in a hot H_3PO_4-line on a Finnigan 251 mass spectrometer at the GMS Laboratory, Department of Geology, University of Bergen.

RESULTS AND DISCUSSION

URANIUM SERIES DATES

Three analyses out of 14 were rejected because of low chemical yields and poorly resolved spectra; the remaining 11 dates are considered to be analytically correct (Table 1). The consistently low U content of LFG 2 (0.045-0.089 ppm U) makes it difficult to perform precise dates, hence the relatively wide age errors. However, in spite of variable errors, the central values of the dates are all in correct stratigraphic order, which permit us to make a tentative age calibration curve by linear interpolation through each dated zone (Fig. 4). This
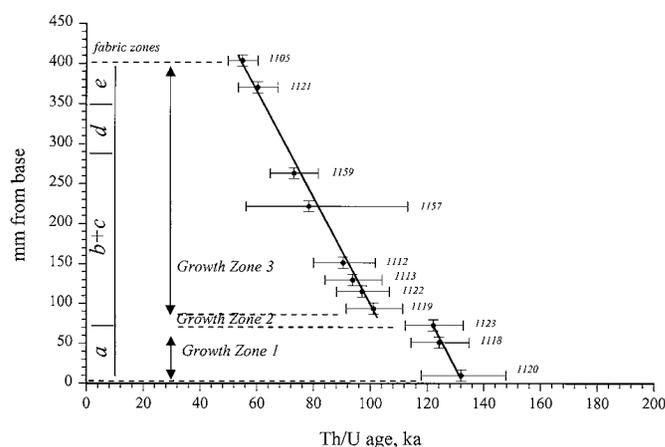
Figure 4. Age-stratigraphy calibration of LFG2. Because there is an apparent break in growth rate, coincident with fabric zone boundary (a/b), the sequence is divided into 3 growth zones. See text for further discussion.
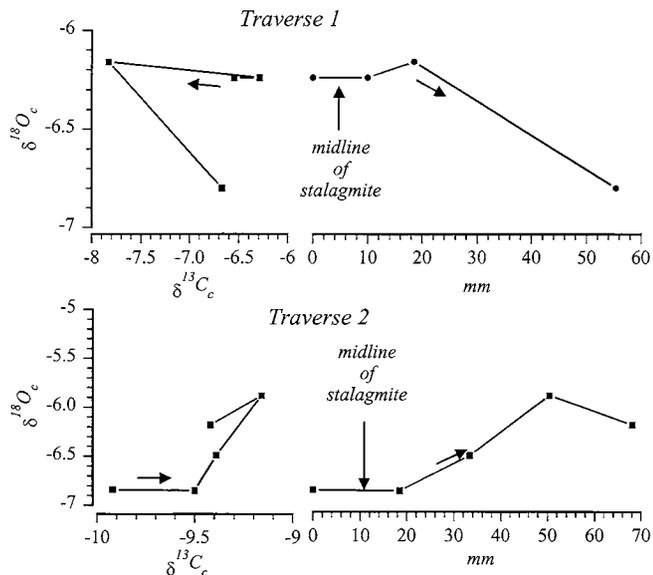
Table 1. Uranium-series dates of stalagmite LFG-2.

Lab No.	Sample	mm from base	(ppm)	$^{234}U/^{238}U$	$^{230}Th/^{234}U$	$^{230}Th/^{232}Th$	age (ka)		Corrected age (ka)	
1120	LFG 2d	0-20	0.072	1.768 ±0.084	0.754 ±0.048	> 1000	131.98	+15.88 -14.14		
1118	LFG 2b	45-55	0.078	1.52 ±0.062	0.718 ±0.034	> 1000	124.21	+10.72 -9.87		
1123	LFG 2h	65-75	0.084	1.66 ±0.073	0.717 ±0.035	> 1000	122.13	+10.66 -9.83		
1119	LFG 2c	85-95	0.085	1.811 ±0.076	0.641 ±0.041	> 1000	101.11	+10.35 -9.58		
1122	LFG 2g	105-115	0.089	1.796 ±0.12	0.624 ±0.04	> 1000	97.10	+9.70 -9.02		
1113	LFG 2f	125-135	0.066	1.725 ±0.156	0.608 ±0.043	> 1000	93.73	+10.42 -9.63		
1112	LFG 2e	145-160	0.072	2.025 ±0.27	0.6 ±0.05	> 1000	90.43	+11.37 -10.46		
1157	LFG 2k	210-230	0.062	1.457 ±0.105	0.65 ±0.073	4	106.01	+20.66 -17.67	78.34	+24.79 -22.03
1159	LFG 2l	250-270	0.045	1.723 ±0.06	0.612 ±0.03	5	94.77	+7.26 -6.87	73.04	+8.69 -8.34
1121	LFG 2x-1	365-375	0.08	2.837 ±0.2	0.448 ±0.041	> 1000	60.33	+7.14 -6.78		
1105	LFG 2x	385-395	0.068	3.63 ±0.27	0.418 ±0.032	> 1000	54.98	+5.33 -5.14		

curve has, of course, rather large errors; we estimate the average error (1 σ) in each age estimate to be ±10-15 ka.

The time span covered by the speleothem growth is the interval (130 ± 15) to (55 ± 15) ka, covering all of oxygen isotope stage 5 (a-e), and some time into stage 4. The marked off-

Traverse 1

midline of stalagmite

Traverse 2

midline of stalagmite

Figure 5. Results of Hendy test on two growth layers (Traverse 1 and 2, Fig. 3). The left diagrams display the covariation of δ18O and δ13C, whereas the diagram on the right side shows progressive changes in δ18O along the growth layer from the apex and down the side of the stalagmite. Arrows indicate the direction from the apex down the sides of the stalagmite. The 20-30 mm wide zone around the apex appears to have grown in isotopic equilibrium, whilst non-equilibrium fractionation might have occurred down the sides of the specimen.

set of the graph between 100 and 120 ka suggests a strong growth attenuation or hiatus somewhere within this time interval, which may coincide with the transition between fabric zones «a» and «b» (Fig. 3). We have therefore divided the sample into 3 growth zones (1-3) (Fig. 4). Even when the chronological error is taken into account, Growth Zone 1 corresponds roughly to the Last Interglacial, (Eemian Stage Se), which occupies only the first 70 mm of the sample. However, the longest growth interval (Growth Zone 3, about 300 mm), corresponds roughly to the remainder of the Early Weichselian (Stage 5a-d) (Mangerud 1989). The growth rates of Zones 1 and 3 appear to be about the same (~7 mm/ka), although the chronological errors do not permit any closer comparison.

HENDY CRITERIA

The Hendy criteria for testing if calcite was precipitated in isotopic equilibrium or not require that there is both no correlation between δ18O and δ13C of successive samples taken along the same growth layer, and that δ18O does not change significantly along the growth layer when traversed across the apex and down the side of the sample. The theory is that, if kinetic fractionation (i.e. non-isotopic equilibrium) occurred during precipitation, δ18O and δ13C would both change in concert as the water film ran off the sides of the stalagmite. If precipitation occurred under isotopic equilibrium, δ18O would largely remain constant, whilst δ13C would change progressively with the traversed path. Since nature is never ideal, a pertinent question is how large tolerance that can be allowed before 'kinetic fractionation' is deduced and the sample regarded as 'useless'. Here, we have followed the standard set by Gascoyne (1992, Fig. 8), i.e. up to about 0.8 per mil change in δ18O is accepted as 'constant' along a single growth layer.

Results of the Hendy test are shown in Figure 5. Neither of the two traverses exceeds 0.8 per mil change in δ18O along each single growth layer traverse. Also, the largest changes
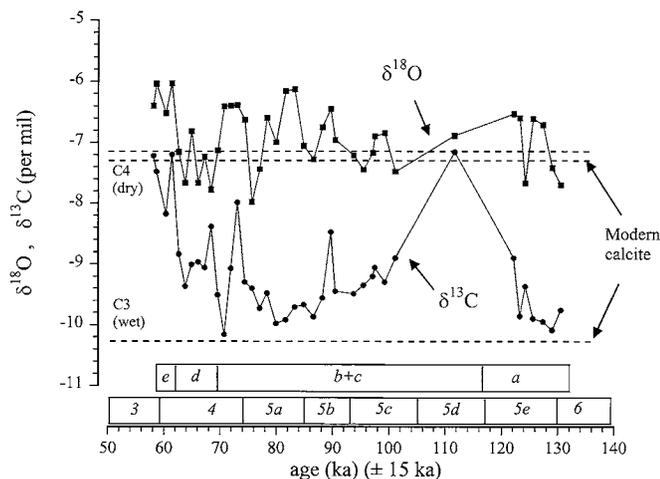
Figure 6. Time-series of oxygen and carbon isotopes in LFG-2 compared to modern values. See text for further discussion. Upper horizontal bar: crystal fabric zones of Figure 3. Lower horizontal bar: oxygen isotope stages.

occur down along the sides of the sample. This is also mirrored in the $\delta^{18}O$ /$\delta^{13}C$ plot. We may therefore conclude that the sample appears to have been precipitated in isotopic equilibrium within 20-30 mm of the apex, but that some fractionation occurred along the sides of the growing stalagmite. The isotopic time-series (which is taken along the growth axis) is thus assumed to represent an equilibrium deposit since it was taken along a line close to the apex where kinetic fractionation effects could not be detected.
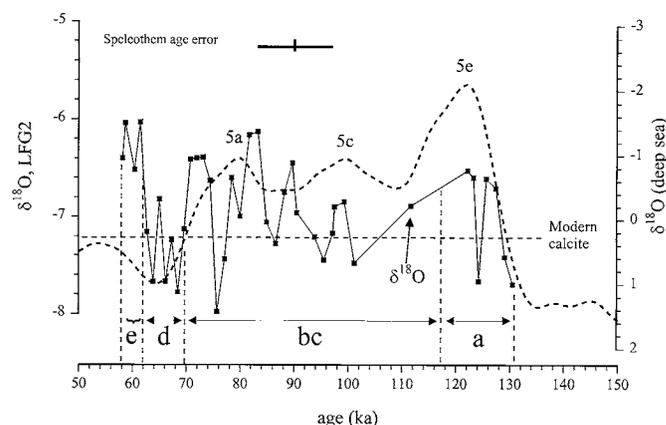
OXYGEN AND CARBON ISOTOPE TIME-SERIES

Along the growth axis, $\delta^{18}O$ and $\delta^{13}C$ vary in the range of [-6 - -8] and [-7 - -10] per mil (VPDB), respectively, which could now be compared with recent isotopic values. Since the sample was no longer growing actively, the isotopic composition of present-day calcite was assessed from four stalactite tips that were taken at the site and analyzed (Table 2). Three of them, which consist of solid, translucent crystals at the apex, have values of $\delta^{18}O$ = -7.21 ±0.11 and $\delta^{13}C$ = -10.3 ±0.04 per mil. The fourth sample, which had a powdery, opaque surface and rather deviant isotopic composition, was rejected.

The age-calibrated time-series of the axial $\delta^{18}O$ and $\delta^{13}C$ profiles are shown in Figure 6. There is some covariation between the two records. For instance, the isotopically light-

est values occur within growth zones 1 and 3. Moreover, both records become isotopically heavier at the top of the sequence (after 50-60 ka), as well as during growth zone 2 (100-120 ka), when deposition ceased or was halted for some time. At the commencement of growth (>130 ka), the $\delta^{18}O$ sequence rises from isotopically lighter to isotopically heavier values than present-day calcite. Also, between 100 and 120 ka, in the slow-growing zone 2, the values drop back to isotopically lighter values than present. Since growth zone 2 represents a period when growth was slow, or even halted, it is reasonable to assume that the climate became cooler and/or drier. These various features of growth and isotopic behavior are taken as roughly corresponding to the rise and fall in temperatures through isotope stage 5e, to the colder stage 5d. Hence, the isotopic response is so that the calcite becomes heavier with increasing temperature, i.e. $\mu > 0$ (equation **[2]**), and we may infer that $\delta^{18}O_w$ variations are dominated by the meteoric signal ($\delta^{18}O_c$) in precipitation.

CORRELATION WITH THE DEEP-SEA RECORD

Due to the large chronological errors, there is, of course, some freedom in the correlation of LFG2 with other records. Also, speleothem records tend to display great temporal resolution, i.e. a rather spiky record of short-term events that are not necessarily present in the smoothed deep-sea curves. Our comparison is therefore somewhat conformistic, i.e. we have tested whether the data, within the freedom given by the timescale, can be brought into harmony with other, known records. For instance, assuming that $\mu > 0$, there is a temperature rise at the beginning of the sequence (120-140 ka) which is in harmony with Termination II, the end of the Penultimate Glaciation (Broecker & van Dunk 1970).

Table 2. Stable isotope values of recent calcite at LFG-2.

Sample (soda straws)	$\delta^{18}O$(VPDB)	$\delta^{13}C$(VPDB)
LFG2-1 (white, fresh)	-7.34	-10.34
LFG2-2 (white, fresh)	-7.22	-10.25
LFG2-3 (white, fresh)	-7.07	-10.29
LFG2-4 (brown, dry)	-6.31	-8.71
Mean (1-3) ± 1σ	-7.21 ±0.110	-10.20 ±0.037

Figure 7. Calibrated isotope time-series of LFG 2 compared with the deep-sea curve of Martinson *et al*. (1987) (thick, dashed curve, oxygen isotope stages 5a, 5c and 5e labeled). The positions of the fabric growth zones of Figure 3 are shown with letters and arrows below the two curves. See text for further discussion.
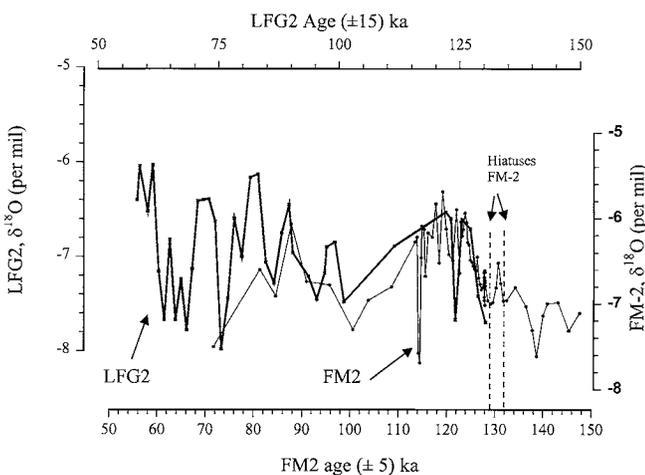
In Figure 7, we have plotted a deep-sea isotope curve that reflects global ice-volume (Martinson *et al.* 1987) and compared it with the LFG2 record. The Last Interglacial, the Eemian (Stage 5e), is recorded within growth zone #1. Albeit represented by only one sample, the record may suggest an intra-Eemian instability (a cold spike at about 122 ka), which is also reported from other speleothem records (Lauritzen 1995; Roberts *et al.* 1998). After about 110 ka, the LFG-2 sequence displays several peaks and troughs, which are difficult (if not impossible) to correlate with corresponding wiggles of the Martinson *et al.* (1987) curve. However, both curves display a distinct drop (cooling and increase in global ice-volume) around 70 ka, which is the Stage 5/4 boundary.

CARBON ISOTOPES AND THE PALEOENVIRONMENT.

During Stage 5b, $\delta^{13}C$ and $\delta^{18}O$ appear to be anticorrelated, while they both show a strong shift towards heavier values at the onset of the Weichselian Glaciation at the Stage 5/4 transition (Fig. 6). If the $\delta^{13}C$ record is interpreted as reflecting changes in the composition of C3 and C4 plants on the surface above the cave, then the 5e/5d transition (growth zone 2) may (shown by only one sample!) represent a period with a higher proportion of C4 plants, i.e. there were drier conditions. Also, at the termination of the sequence (the Stage 5/4 transition), the isotopic record displays a similar C3-C4 shift, but the corresponding oxygen isotope shift suggests that it also became warmer as well as drier.

CORRELATION WITH OTHER SPELEOTHEM RECORDS

In Figure 8, we have compared the LFG2 record with the FM2 record from northern Norway (Lauritzen 1995). There is a remarkable correlation between the two series. Both display a rapid rise in $\delta^{18}O$ at Termination II (*ca.* 130 ka). Both sequences display a cold spike, although the imprecise chronology does not permit us to determine if the spikes are exactly the same age. It is, however, interesting to note that after FM2 ceased to grow at 70 ka and displayed a cooling signal, LFG-2 continues to grow while its stable isotope record suggests a warmer and drier climate in northwest Romania. This is compatible with the expansion of the Scandinavian ice sheets in concert with the dry, glacial steppe environment in central and southern Europe.

CONCLUSIONS

The LFG-2 stalagmite from northwest Romania grew through oxygen isotope Stage 5-4, and possibly also some time into Stage 3. Albeit a rather low uranium content and, thus, imprecise chronology, the stable isotope signal correlates quite well with speleothem record (FM-2) from northern Norway and broadly with the marine record. Termination II is well defined in the record, and during oxygen isotope Stage 5e (the Eemian, or the last Interglaciation in Europe), the temperature was higher than today. Less abundant data suggests that during Stage 5d, cooling occurred, accompanied with slow or no speleothem growth, as well as $\delta^{13}C$ shifts that may indicate a C4 vegetation (i.e. drier). Near the end of the sequence, probably after the isotope Stage 5/4 transition, temperature increased, growth slowed down, and C4 plants dominated. This might be interpreted as commencement of warmer and drier conditions at the onset of the Weichselian glaciation. These events are summarized in Table 3.

ACKNOWLEDGMENTS

Figure 8. The oxygen isotope record of LFG6 (thick curve) compared with the α-dated last interglacial (thin curve with dots) from Northern Norway, FM2 (Lauritzen 1995). The main isotopic warming in the Eemian, around 120 ka, is present in both sequences, and demonstrates that speleothem climatic signals can be correlated over large latitudinal distances.

Table 3. Summary of climatic changes during the growth of LFG-2.

Isotope stage	Response in LFG-2	FM-2 (North Norway)	Scandinavian Glaciation
6	No growth	Growth commenced	Saalian glaciation
6/5e	rapid warming	rapid warming	Termination II
5e	warm, unstable	warm, unstable	The Eemian
5d	cold, dry, slow growth/hiatus?	slow growth	Cold, glacier expansion
5a-5c	rapid growth	slow growth	Brørup/Odderade interstadials
4	warm, dry, then hiatus	corrosional hiatus	Middle Weichselian glaciation

Mike Talbot are thanked for useful comments and language corrections. This is the 3rd contribution to the SPEP III program in Romania and contribution No.35 to the Karst Research Project in Norway.

REFERENCES.

Baker, A., Smart, P.L., Edwards, R.L. & Richards, D.A. (1993a). Annual growth banding in a cave stalagmite. *Nature 364*: 518-520.

Baker, A., Smart, P.L. & Ford, D.C. (1993b). Northwest European palaeoclimate as indicated by growth frequency variations of secondary calcite deposits. *Palaeogeography Palaeoclimatology Palaeoecology 100*: 291-301.

Bar-Matthews, M. & Ayalon, A. (1997). Late Quaternary paleoclimate in the eastern Mediterranean region from stable isotope analysis of speleothems at Soreq Cave, Israel. *Quaternary Research 47*: 155-168.

Bastin, B. (1978). L'analyse pollinique des stalagmites: Une nouvelle possibilité d'approche des fluctuations climatiques du quaternaire. *Annales de la Societé Geologique de Belgue 101*: 13-19.

Broecker, W.S. & van Dunk, J. (1970). Insolation changes, ice volumes, and the 180 record in deep-sea cores. *Reviews of Geophysics and Space Physics 8*: 169-198.

Craig, H. (1961). Isotopic variation in meteoric waters. *Science 133*: 1702-1703.

Dansgaard, W. (1964). Stable isotopes in precipitation. *Tellus 16*: 436-468.

Diaconeasa, B., Clichici, O. & Dragos, I. (1976). Quelques renseignements sporopoffiniques concernant le passé de la vegetation Quarternaire de Transylvanie. *Contributii botanice*: 193-196.

Dickson, J.A.D. (1993). Crystal growth diagrams as an aid to interpreting the fabrics of calcite aggregates. *Journal of Sedimentary Petrology 63*: 1-17.

Dulinski, M. & Rozanski, K. (1990). Formation of $^{13}C/^{12}C$ isotope ratios in speleothems: A semi-dynamic model. *Radiocarbon 32*: 7-16.

Folk, R. & Assereto, R. (1976). Comparative fabrics of length-slow and length-fast calcite and calcitized aragonite in a Holocene speleothem, Carlsbad Caverns, New Mexico. *Journal of Sedimentary Petrology 56*: 486-496.

Gascoyne, M. (1992). Palaeoclimate determination from cave calcite deposits. *Quaternary Science Reviews 11*: 609-632.

Gascoyne, M., Schwarcz, H.P. & Ford, D.C. (1983). Uranium-series ages of speleothem from northwest England correlation with Quaternary Climate. *Philosophical Transactions of The Royal Society of London Series B 301*: 143-164.

Gat, J.R. (1980). The isotopes of hydrogen and oxygen in precipitation. In Fritz, P. & Fontes, J.C. (eds.) *Handbook of Environmental Isotope Geochemistry*. Elsevier Scientific Publishing Company, Amsterdam: 21-48.

Genty, D. & Quinif, Y. (1996). Annually laminated sequences in the internal structure of some Belgian stalagmites - importance for palaeoclimatology. *Journal of Sedimentary Research 66*: 275-288.

Gordon, D., Smart, P.L., Ford, D.C., Andrews, J.N., Atkinson, T.C., Rowe, P.J. & Christopher, N.S.J. (1989). Dating of late Pleistocene interglacial and interstadial periods in the United Kingdom from speleothem growth frequency. *Quaternary Research 31*: 14.26.

Grgor'ev, D.P. (1965). *Ontogeny of Minerals.* Israel Program for Scientific Translations, Jerusalem: 250p.

Hendy, C.H. (1971). The isotopic geochemistry of speleothems. Part 1. The calculation of the effects of different modes of formation on the isotopic composition of speleothems and their applicability as paleoclimatic indicators. *Geochimica et Cosmochimica Acta 35*: 801-824.

Holingren, K., Lauritzen, S.-E. & Possnert, G. (1994). $^{230}Th/^{234}U$ and ^{14}C dating of a late Pleistocene stalagmite in Lobatse II Cave, Botswana. *Quaternary Geochronology 13*: 111-119.

Holmgren, K., Karlén, W. & Shaw, P.A. (1995). Paleoclimatic significance of the stable isotope composition and petrology of a late Pleistocene stalagmite from Botswana. *Quaternary Research 43*: 320-328.

Holingren, K., Karlén, W., Lauritzen, S.-E., Lee-Thorp, J., Partridge, T.C., Piketh, S., Repinski, P., Stevenson, C., Svanerd, O. & Tyson, P.D. (in review). A high-resolution reconstruction of the palaeoclimate of the north-eastern summer rainfall region of South Africa over the last three millennia. *The Holocene.*

Jarai-Komlodi, M. (1991). Late Pleistocene vegetation history in Hungary since the last interglacial. In Pecsi, M. and Schweitzer, F. (eds.) *Quaternary Environments in Hungary, Studies in Geography in Hungary, 26.* Akademiai Kiado, Budapest: 5-46.

Kendall, A.C. & Broughton, P.L. (1978). Origin of fabrics in speleothems composed of columnar calcite crystals. *Journal of Sedimentary Petrology 48*: 519-538.

Latham, A.G. & Schwarcz, H.P. (1992). Carbonate and sulphate precipitates. In Ivanovich, M. & Harmon, R.S. (eds.). *Uranium-series Disequilibrium: Applications to Earth, Marine, and Environmental Sciences.* Clarendon Press, Oxford: 423-459.

Latham, A. G., Schwarcz, H.P. & Ford, D.C. (1979). Palaeomagnetism of stalagmite deposits. *Nature 280*: 383-385.

Latham, A.G., Ford, D.C., Schwarcz, H.P. & Birchall, T. (1989). Secular variation from Mexican stalagmites: their potential and problems. *Physics of the Earth and Planetary Interiors 56*: 34-48.

Lauritzen, S.-E. (1993a). *"Age4U2U". Program for reading ADCAM energy spectra, integration peak-correction and calculation of $^{230}Thorium/^{234}Uranium$ ages.* Computer Program Turbo Pascal Code, 5,000 lines, Department of Geology, Bergen.

Lauritzen, S.-E. (1993b). Natural Environmental Change in Karst: The quaternary record. *Catena Supplement 25*: 21-40.

Lauritzen, S.-E. (1995). High-resolution paleotemperature proxy record during the last interglaciation in Norway from speleothems. *Quaternary Research 43*: 133-146.

Lauritzen, S.-E. (1996). Calibration of speleothem stable isotopes against historical records: A Holocene temperature curve for north Norway? *Karst Waters Institute Special Publication 2*: 78-80.

Lauritzen, S.-E. (1998). "SPEP": the speleothem record in the Pole-Equator-Pole transects. In Gasse, F., Kroeplin, S. & Oldfield, F. (Eds.) *PEP III: The Pole-Equator-Pole transect through Europe and Africa ["Coordinating paleoenvironmental research along the PEP III transect" Bierville (France), September 12-15 1996].* PAGES, Bern: 37-43.

Lauritzen, S.-E. & Lundberg, J. (1998). Rapid temperature variations and volcanic events during the Holocene from a Norwegian speleothem record. *PAGES Open Science Meeting, University of London, April 20-23, 1998*: 88.

Lauritzen, S.-E., Ford, D.C. & Schwarcz, H.P. (1986). Humic substances in speleothem matrix- Paleoclimatic significance.

Proceedings, 9th International Speleological Congress. Barcelona 1: 77-79.

Lauritzen, S.-E., Løvlie, R., Moe, D. & Østbye, E. (1990). Paleoclimate deduced from a multidisciplinary study of a half-million-year-old stalagmite from Rana, northern Norway. *Quaternary Research 34*: 306-316.

Lauritzen, S.-E., Hercman, H. & Glazek, J. (1996). Preliminary comparison between Norwegian and Polish speleothem growth frequencies. *Karst Waters Institute Special Publication 2*: 81-83.

Mangerud, J. (1989). Correlation of the Eemian and the Weichselian with deep sea oxygen isotope stratigraphy. *Quaternary International 3/4*: 1-4

Martinson, D.G., Pisias, N.G., Hays, J.D., Imbrie, J., Moore, T.C. & Shackleton, N.J. (1987). Age dating and the orbital theory of the Ice Ages: Development of a high-resolution 0 to 300,000 yr chronostratigraphy. *Quaternary Research 27*: 1-29.

Onac, B.P. (1996). Mineralogy of speleothems from caves in Padurea Craiului Mountains (Romania), and their palaeoclimatic significance. *Cave and Karst Science 23*: 109-124.

Onac, B.P. & Lauritzen, S.-E. (1996). The climate of the last 150,000 years recorded in speleothems: preliminary results from north-western Romania. *Theoretical and Applied Karstology 9*: 9-21.

Onac, P.B. & Lauritzen, S.-E. (1996). Pleistocene and Holocene climate in north-western Romania as indicated by growth frequency variations of speleothems. In: Horoi, V. & Constantin, S. (Eds.) *The XIVth International Symposium on Theoretical and Applied Karstology. Baile Herculane - Romania, May 26- June 1, 1996*. Institul de Spéologie "Emil Racovita", Bucarest: 42.

Pécsi, M. (1993). *Quaternary and Loess Research Akadémiai.* Kiadó, Budapest: 20-36.

Perkins, A.M. & Maher, B.A. (1993). Rock magnetic and palaeomagnetic studies of British speleothems. *Journal of Geomagnetism and Geoelectricity 45*: 143-153.

Ramseyer, K., Miano, T., D'Orazio, V., Wildberger, A., Wagner, T. & Geister, J. (1997). Nature and origin of organic matter in carbonates from speleothems, marine cements and coral skeletons. *Organic Geochemistry 26*: 361-378.

Roberts, M.S., Smart, P.L. & Hawkesworth, C.J. (1998). Evidence for an intra-Eemian cooling event from TIMS [230]Th/[234]U dating of a British stalagmite (Abstract). *PAGES Open Science Meeting, University of London, April 20-23, 1998*: 109-110.

Rowe, P.J., Dennis, P.F., Atkinson, T.C., Lauritzen, S.-E. & Lundberg, J. (1998). A high resolution deuterium record from fluid inclusions in a late Holocene speleothem from S.W. Britain. *PAGES Open Science Meeting, University of London, April 20-23, 1998*: 112.

Schwarcz, H.P. (1986). Geochronology and isotope geochemistry in speleothems. In Fritz, P. & Fontes, J., (eds.) *Handbook of Environmental Isotope Geochemistry*. Elsevier, Amsterdam: 271-303.

Schwarcz, H.P. & Yonge, C. (1983). Isotopic composition of pale-owaters as inferred from speleothem and its fluid inclusions. In *Paleoclimates and Paleowaters; a Collection of Environmental Isotope Studies*. International Atomic Energy Agency Vienna Austria.

Shopov, Y., Ford, D.C. & Schwarcz, H.P. (1994). Luminescent microbanding in speleothems: High-resolution chronology and paleoclimate. *Geology 22*: 407-410.

Shopov, Y., Tsankov, L.T., Yonge, C.J., Krouse, H.P.R. & Jull, A.J.T. (1997). Influence of the bedrock CO_2 on stable isotope records in cave calcites. *Proceedings of the 12th International Congress of Speleology 1*: 65-68.

Talma, A.S. & Vogel, J.C. (1992). Late Quaternary paleotemperatures derived from a speleothem from Cango Caves, Cape Province, South Africa. *Quaternary Research 37*: 203-213.

Talma, A.S., Vogel, J.C. & Partridge, T.C. (1974). Isotopic contents of some Transvaal speleothems and their palaeoclimatic significance. *South African Journal of Science 70*: 135-140.

Tamas, T. & Vremir, M. (1997). Karstological investigations in the Middle Basin of Lada Valley (Padurea Craiului Mountains, Romania). *Proceedings of the 12th International Congress of Speleology, La Chaux-de-Fonds, Switzerland 1*: 413-416.

Urban, B. (1984). Palynology of Central European loess-soil sequences: 229-248. In Pecsi, M. (ed.) *Lithology and Stratigraphy of Loess and Paleosols*. Geographical Research Institute, Hungarian Academy of Science, Budapest.

Vremir, M. (1994). Pesteri descoperite prin lucrari industriale în bazinul Mijlociu al Vaii Iadei (Muntii Padurea Craiului). *Ardealul Speologic 4*: 30-57.

Willis, K.J. (1994). The vegetational history of the Balkans. *Quaternary Science Reviews 13*: 769-788.

ERRATUM

The editor wishes to correct a typesetting error in the paper by Toth in the December issue (v. 60, n. 3) of the *Journal of Cave and Karst Studies*. On page 169, first paragraph, the first full sentence should read: "These fast flow rates (1.67×10^{-3} m/sec for the first test and 1.67×10^{-2} m/sec for the second)…." The parenthetical statement in the last sentence of the same paragraph should read: "(4.32×10^{-3} m/sec through 70 m of overburden)." We thank Bill Mixon for noting our error.

Book Review

Global Karst Correlation (IGCP 299)
Yuan Daoxian and Liu Zaihua (eds.) (1998). Science Press Beijing and VSP Utrecht: 308 pp., 69 pictures (19 b/w), 4 Appendices.

This book represents the final report of the International Geological Correlation Program (UNESCO/IUGS), Project 299 (IGCP299): Geology, climate, hydrology and karst formations.

Chapter 1 deals essentially with the basic ideas, methodologies and major results of the IGCP 299. After a short background presentation the goals of this project are highlighted as follows:

• to identify the global differences in karst features that appear on various geological, hydrological and climatic settings, and to clarify the regularities of their distribution;

• to reconstruct the palaeoenvironment and palaeoclimate changes from karst records;

• management of karst areas (evaluation, prediction, exploitation of natural resources) and environmental protection of various karst areas.

Chapter 2 deals specifically with the basic physical and chemical principles determining karstification in both the initial and the mature state of karst. The aim of this chapter is to underline the reasons for which karst landscapes developed on different geo-morphoclimatic regions, which results in such a large variety of forms and features. In order to accomplish this goal, the authors discuss several physico-chemical models showing how karst processes are driven by chemical, physical and hydrogeologic forces.

Chapters 3 through 14 offer up-to-date coverage on various karst aspects concerning some of the most important karst regions of the world (China, Great Britain, eastern United States, Slovenia, Romania, Japan, Vietnam, Australia and New Guinea, Ural Mountains, Brazil, Spitsbergen and the Baltic Republics). For each of these regions, the authors emphasize their particular geology and hydrogeology as well as many extensive updated and critically evaluated Quaternary climatic data inferred from cave deposits. Worked examples, both fundamental and applied, presented alongside numerous figures and tables, make the text clear and concise. Most chapters include expanded and in-depth treatment of subjects such as resources and environmental problems in karst areas.

Chapter 15 provides an extensive presentation of high-resolution records of climatic variations and solar forcing inferred from the luminescence of speleothems. Based on analyses performed on samples from three caves (Coldwater, USA; Rats Nest, Canada; and Duhlata, Bulgaria) the authors stress that the temporal resolution of the method is 10^3-10^4 times greater than any other used so far for terrestrial paleoclimatic reconstruction.

The final chapter of the book presents a few perspectives for karst science, including the application of earth system science in karst studies, karst proxies used for global change studies, karst development on different environments and sustainable development for various karst environmental systems.

In short, this book is a comprehensive, updated overview of several well-known karst regions of the world that provides an impressive informational database. This will enable scientists to perform geomorphologic, hydrologic and climatic correlations throughout different karst regions on the Earth.

Reviewed by: Bogdan Petroniu Onac, A7 Materials Research Laboratory, The Pennsylvania State University, University Park, PA 16802-4801, bonac@bioge.ubbcluj.ro

---

Shannon Knapp
Shannon grew up in San Diego, California. She majored in Biology at American University in Washington, DC, where she began caving and studying cave critters with Dan Fong. Shannon is currently studying terrestrial salamanders for her MS in Wildlife at Virginia Tech, and occasionally still gets underground in West Virginia.

Daniel Fong
Dan has been working on various aspects of cave biology since 1980. He received his PhD at Northwestern University where he worked with Dave Culver. He is currently Associate Professor of Biology at American University, where he conducts research on the ecology and evolution of cave organisms.

Louise D. Hose, PhD, directs the Environmental Studies Program at Westminster College in Fulton, Missouri. A geologist, she has explored and studied caves in Mexico for over 25 years. She currently coordinates the scientific investigations for the NSS's Caves of Tabasco Project.

James A. Pisarowicz, PhD, is a park ranger at Wind Cave National Park in Hot Springs, South Dakota. He is a Lew Bicking Awardee, NSS Fellow, and is the director of the NSS's Caves of Tabasco Project.

Stein-Erik Lauritzen is associate professor of geology at the University of Bergen, Norway, but was first educated as an organic synthetic chemist. However, since the early 1970s he has been interested in caves and caving and has done cave-related research (apart from Norway) in North America, the Caribbean, central and eastern Europe, Spitsbergen, China and Australia. He is running a uranium-series dating and isotope laboratory in Bergen, and his main interests are the use of speleothem and cave sediment stratigraphy in paleoclimatic research, cave geomorphology and speleogenesis, as well as environmental aspects of karst.

Dr. Bogdan P. Onac is an Associate Professor in the Department of Mineralogy, University of Cluj (Romania), where he teaches crystallography and karstology. He also holds an appointment as a senior researcher at the Speleological Institute "Emil Racovita" (Cluj) of the Romanian Academy of Sciences. His fields of interest are cave mineralogy and crystallography as well as reconstruction of Quaternary paleoclimate and paleoenvironment based on speleothems.

Vulcanospeleological Special Session sponsored by the NSS Geology and Geography Section

Call for contributions:

During the 1999 National Speleological Convention July 12-16th in Filler, Idaho, a Special Session is planned to cover concepts and exploration results in the rapidly developing field of Vulcanospeleology.

The session will start with lunch, Monday the 12th. A keynote speaker, tentatively Dr. Ron Greeley from the Arizona State University and one of the most eminent planetologists and cavers will open the afternoon session. The rest of the afternoon will be devoted to theme-contributions, reviewing specific aspects of vulcanospeleology. In the evening there is the Howdy Party during which Peter Fonda's "Idaho Transit" will be screened, a cult SF film featuring the lava landscape of Idaho's Crater of the Moon National Park. The morning session on Tuesday, the 13th of July, will be devoted to oral open topic presentations, covering recent discoveries of lava cave research. Posters can be displayed during the Geology & Geography Poster Session on Monday morning.

Chairpersons: Dr. W.R. Halliday, Dr. Stephan Kempe

Abstracts, not longer than 250 words, should be directed prior to May 21st to Dr. Stephan Kempe; Geological-Paleontological Institute; Techn. Univ. Darmstadt; Schnittspahnstr. 9; D-64807 Darmstadt; Germany; email: kemp@bio.tu-darmstadt.de Fax: 49 6151 16 6539 ; Tel.: 49 6151 16 2471.

Call for Geology and Geography Papers

The NSS Section of Cave Geology is accepting abstracts of papers for presentation at the Geology Session of the 1999 NSS Convention, to be held in Filer, Idaho, from 12-16 July 1999. Abstracts should be no more than 250 words in length (this limit must be strictly met). In addition to the text, the abstracts should contain the title of the paper, and the name(s) and address(es) of the author(s). The abstracts should be informative summaries that include the conclusions, and not lists of topics that "...will be discussed." Bibliographies and references should not be given in the abstracts. Papers may be submitted for either oral presentation as a poster.

Send any questions and your abstracts by mail, e-mail, disk, or fax to:George Veni; 11304 Candle Park; San Antonio, Texas 78249-4421; 210-558-4403 (phone and fax, but you must call before faxing); gveni@flash.net

The deadline for abstracts is 21 May 1999. Early submissions are encouraged. Confirmation notes will be sent to everyone sending an abstract.

Karst Modeling: A Symposium for Karst Professionals

An international symposium on Karst Modeling, held in Charlottsville, VA, February 24-27, 1999, allowed scientists and practitioners to cross traditional disciplinary boundaries to discuss conceptual, analytical, digital, scale, and statistical models for karstic aquifers. There were 108 participants, including guests from Australia, Canada, Germany, Switzerland, and Guam.

Karst hydrology seems poised on the edge of a major advance. In the very early days, carbonate aquifers were tested and characterized by the same methods (mostly by drilling wells) and by the same models as aquifers in other kinds of rocks. In the 1970s, the importance of conduit systems became recognized and for the next 10-20 years, karst aquifer investigations focused on tracer tests, groundwater basin delineation, spring hydrographs, and other measures of the conduit system. Now, in the decade of the 90s, the emphasis is in putting it all together. Conduits are important, surface water/groundwater interactions are important, fracture and matrix flow is important. The current generation of models attempts to put all these aspects of the aquifer together.

Presentations at the meeting covered the entire range of modeling problems including the geochemical evolution of aquifer properties; groundwater flow mechanics in conduits and fractures, and their interactions; contaminant transport; and improvements in the technology of water tracing and groundwater basin delineation. A general model for karst aquifers is a formidable problem, but there was a sense of optimism that a model can be found.

The Karst Waters Institute organized the meeting with funding from the National Science Foundation, the Army Research Office, the American Chemical Society, and the Cave Conservancy of the Virginias. A 265-page proceedings was published; it is available from KWI, R.R. #1, Box 527, Petersburg, PA 16669-9211 for $40.00 postpaid.

Elizabeth White

Conference on Microbial Marks in Mineralization

A Society of Economic Paleontologists and Mineralogist research conference on Microbial Marks on Mineralization will be held in November 1999 at the Bahamian Field Station on San Salvadore Island. To add your name to the mailing list, contact: Dawn Sumner - sumner@geology.ucdavis.edu.

National Speleological Society
2813 Cave Avenue
Huntsville, Alabama 35810-4431